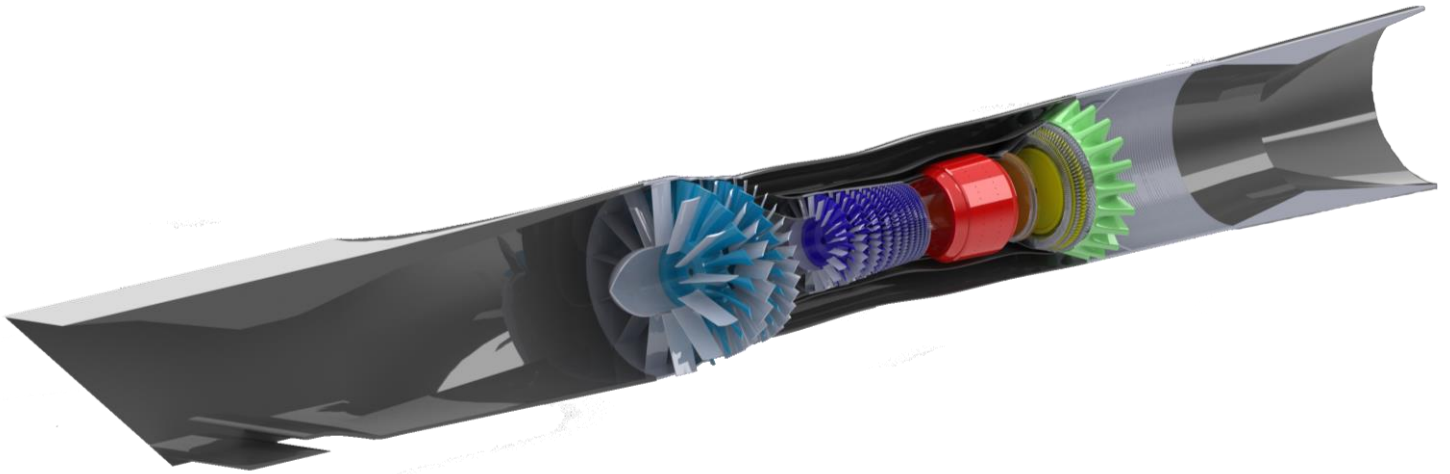


CE18-Bullet: Candidate Engine for a Next Generation Supersonic Transport



Team Members:

Brady Behymer

Brendan Disque

Garett Foster

Collin Green

Jacob Niles

Blake Stapp

Mouhamed Thiam

Schuyler Trenary

Bret Valenzuela

Jordan Wilson

Faculty Advisor:

Dr. Kurt Rouser



AIAA Undergraduate Aircraft Engine
Design Competition 2017/18

Team Members:

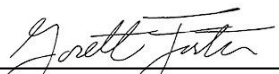
Brady Behymer
906390



Brendan Disque
737288



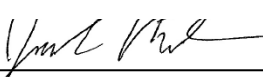
Garett Foster
878900



Collin Green
922139



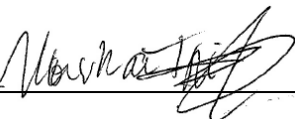
Jacob Niles
922147



Blake Stapp
517978



Mouhamed Thiam
807605



Schuyler Trenary
922122



Bret Valenzuela
739416



Jordan Wilson
890843



Dr. Kurt Rouser
114100
Faculty Advisor



Abstract

This report details the cycle and component design of a gas turbine engine to be used on a 100 passenger supersonic transport. The engine, CE18-Bullet, is a mixed-flow, low-bypass ratio turbofan with a max diameter at the fan of 89 inches and a bypass ratio of 2.1. The fan pressure ratio is 2.5 and core of the engine has a 10-stage compressor, which achieves an overall pressure ratio of 42. The low pressure shaft powers the fan using 2 turbine stages while the high pressure shaft powers the compressor using 2 turbine stages. The advanced design of this engine demonstrates substantial improvements over a previously designed baseline engine in TSFC, thrust, weight, and flight envelope. The CE18-Bullet engine provides an 18.1% improvement of TSFC and a 34.2% improvement on thrust at the cruise condition.

| <i>General Characteristics</i> | |
|--|-------------|
| Wing Area (ft ²) | 4096 |
| Max Takeoff Weight | 317499 |
| Takeoff Thrust (required) | 64625 |
| <i>Performance</i> | |
| Max Speed (kts) | 1742 |
| Cruise speed (kts) | 1550 |
| Mission Fuel Burn (lbs) | 61804 |
| Cruise TSFC (lbm/hr)/lbf | 0.894 |
| Takeoff TSFC (lbm/hr)/lbf | 0.613 |
| Engine Weight (lbs) | 11,084 |
| Fan Diameter (in) | 89 |
| <i>Trade Studies</i> | Page # |
| Aircraft Constraint Diagram | 42 |
| Engine Cycle Design Space Carpet Plots | 4 |
| In-Depth Cycle Summary | 10 |
| Final Engine Flowpath | 40 |
| Final Cycle Study Using Chosen Cycle Program | 7 |
| Turbomachinery Design Information (Fan, HPC, LPT, HPT) | 16,19,28,28 |
| First Stage Velocity Triangles (Fan, HPC, LPT, HPT) | 18,20,31,31 |
| Inlet and Nozzle Performance (Inlet, Nozzle) | 14, 39 |

| <i>Summary Data</i> | |
|--|-------|
| Design MN | 1.6 |
| Design Altitude (ft) | 52500 |
| Design Fan Mass Flow (lbm/s) | 600 |
| Design Gross Thrust (lbf) | 48472 |
| Design Bypass Ratio | 2.1 |
| Design Net Thrust (lbf) | 19703 |
| Design TSFC (lbm/hr)/lbf | 0.894 |
| Design Overall Pressure Ratio | 42 |
| Design T4.1 (deg R) | 3400 |
| Design Engine Pressure Ratio | 1.005 |
| Design Fan Pressure Ratio | 2.5 |
| Design Chargeable Cooling Flow (%@25) | 5 |
| Design Non-Chargeable Cooling Flow (%@25) | 5 |
| Design Adiabatic Efficiency for Each Turbine | 0.90 |
| Design Polytropic Efficiency for Each Compressor | 0.91 |
| Design HP Shaft RPM | 8116 |
| Design LP Shaft RPM | 4422 |
| <i>Additional Information</i> | |
| Design Shaft Off-Take Power (HP,LP) | 100 |
| Design Customer Bleed Flow (%) | 1 |

Table of Contents

| | |
|---|-----|
| Abstract..... | iii |
| Introduction..... | 1 |
| 1.0 Cycle Analysis | 1 |
| 1.1 Design Approach | 2 |
| 1.2 Cycle selection | 2 |
| 1.3 Baseline AEDsys validation..... | 3 |
| 1.4 New Engine Design | 3 |
| 1.4.1 On-Design Analysis | 4 |
| 1.4.2 Off-Design Analysis | 7 |
| 1.6 Mission and Fuel Burn Analysis..... | 8 |
| 1.7 Other CE18 Bullet Analysis..... | 9 |
| 1.7.1 Weight Analysis..... | 9 |
| 1.7.2 Noise Analysis | 9 |
| 1.7.3 NOx Analysis..... | 10 |
| 1.8 Cycle Design Summary | 10 |
| 2.0 Supersonic Inlet Design | 11 |
| 2.1 Inlet Type Selection | 11 |
| 2.2 Inlet Sizing..... | 11 |
| 2.3 Inlet Off-Design Performance..... | 13 |
| 2.4 Inlet Bleed Flow..... | 14 |
| 2.5 Inlet Diffuser | 14 |
| 2.6 Inlet Drag | 15 |
| 2.7 Inlet Model..... | 15 |
| 3.1.0 Fan | 16 |
| 3.1.1 Inlet Guide Vane | 17 |
| 3.1.2 Fan Stage and Blade Design | 17 |
| 3.1.3 Fan Model | 19 |
| 3.2.1 HPC Stage Design..... | 20 |
| 3.2.2 HPC Blade Design | 21 |
| 3.2.3 HPC Structural Analysis | 22 |
| 3.2.4 HPC Overall..... | 23 |
| 3.2.5 Compressor Model..... | 23 |
| 4.0 Combustion System Design | 24 |
| 4.1 Diffuser Design..... | 25 |

| | |
|---|----|
| 4.2 Rich Burn – Quick Mix – Lean Burn (RQL) | 25 |
| 4.3 Materials and Cooling Methods | 26 |
| 4.4 Combustor Geometry | 27 |
| 4.5 Fuel Injection Technique & Ignition Source..... | 27 |
| 4.6 Combustor Model | 27 |
| 5.0 Turbine Design..... | 28 |
| 5.1 Turbine Design Analysis and Approach | 28 |
| 5.2 Turbine Flow Calculations..... | 30 |
| 5.3 Turbine Aerothermodynamic Calculations | 32 |
| 5.4 Blade Design..... | 33 |
| 5.5 Turbine Material Selection..... | 34 |
| 5.6 Stress Considerations | 35 |
| 5.7 Turbine Model | 36 |
| 6.0 Mixer Design | 36 |
| 7.1 Nozzle Type Selection | 37 |
| 7.2 Nozzle Sizing | 38 |
| 7.3 Nozzle Design Results | 38 |
| 7.4 Afterburner Design | 39 |
| 7.5 Exhaust System Model | 39 |
| 8.0 CE18-Bullet Flowpath | 40 |
| 9.0 Engine Subsystems | 40 |
| 9.1 Auxiliary Power Unit and startup | 40 |
| 9.2 Fuel System..... | 40 |
| 9.3 Engine Control | 40 |
| 9.4 Bearing..... | 40 |
| 10.0 Design Summary and Considerations | 41 |
| 11.0 Constraint Diagram | 42 |
| 12.0 CE18-Bullet Full Engine Model | 43 |
| 13.0 References..... | 44 |

List of Figures

| | |
|--|-------------------------------------|
| Figure 1.1 NASA N+2 Supersonic Transport Concept..... | 1 |
| Figure 1.2 AEDsys Performance Results for RFP Basline Engine..... | 3 |
| Figure 1.3 Solution Space Carpet Plots for CE18-Bullet..... | 4 |
| Figure 1.4 Selected Solution Space for CE18-Bullet..... | 5 |
| Figure 1.5 AEDsys On-Design Performance Results for CE-18 Bullet | 6 |
| Figure 2.1 Subcritical inlet operation..... | 12 |
| Figure 2.2 Pressure Recovery with Varying Inlet Angles at Cruise Condition | 12 |
| Figure 2.3 Supersonic Inlet Geometry | 13 |
| Figure 2.4 Off-Design Inlet Performance with Ramp Scheduling..... | 14 |
| Figure 2.5 Supersonic Inlet CAD Model | 15 |
| Figure 3.1 Fan/Compressor Velocity Triangle Nomenclature..... | 16 |
| Figure 3.2 Fan Airfoil and Twist | 18 |
| Figure 3.3 Fan CAD Model | 19 |
| Figure 3.4 Blade Incidence and Deviation Angles..... | Error! Bookmark not defined. |
| Figure 3.5 Compressor Airfoil and Twist | 22 |
| Figure 3.6 Compressor CAD Model..... | 23 |
| Figure 4.1 RQL combustor | 24 |
| Figure 4.2 Effect of Splitter Veins | 25 |
| Figure 4.3 Cooling Effectiveness..... | 26 |
| Figure 4.4 CO and NOx Emissions..... | 26 |
| Figure 4.5 Annular Combustor CAD Model | 27 |
| Figure 5.1 Turbine Velocity Triangle Nomenclature..... | 28 |
| Figure 5.2 Turbine (HPT and LPT) CAD Model..... | 36 |
| Figure 7.1 Gross Thrust Coefficient contour plot..... | 38 |
| Figure 7.2 Nozzle On-Design Cross Section | 38 |
| Figure 7.3 Afterburner and Nozzle CAD Model | 39 |
| Figure 8.1 CE18-Bullet Flowpath..... | 40 |
| Figure 11.1 Constraint Diagram..... | 42 |
| Figure 12.1 CE18-Bullet Exploded View | 43 |
| Figure 12.2 CE18-Bullet Drawing with Major Dimensions | 43 |

List of Tables

| | |
|---|-------------------------------------|
| Table 1.1 Baseline Engine Performance Values + 5% reduction in TSFC..... | 2 |
| Table 1.2 CE18-Bullet Component Efficiencies..... | 3 |
| Table 1.3 Design Parameter Performance Trends..... | 5 |
| Table 1.4 CE18-Bullet Cycle Design..... | 6 |
| Table 1.5 Off-Design Performance Results and Comparison to Baseline | 7 |
| Table 1.6 CE18-Bullet Cycle Efficiencies..... | 8 |
| Table 1.7 Fuel Burn Analysis | 8 |
| Table 2.1 Inlet On-Design Performance Values | 13 |
| Table 3.1 Guidelines on Range of Compressor Parameters..... | 16 |
| Table 3.2 Fan and Inlet Guide Vane | 17 |
| Table 3.3 Fan Velocity Triangle and Aerothermodynamic Calculations..... | 18 |
| Table 3.4 Fan Geometry | 18 |
| Table 3.5 Compressor and Inlet Guide Vane Parameters | 19 |
| Table 3.6 Compressor Velocity Triangle and Aerothermodynamic Calculations | 20 |
| Table 3.7 Compressor Dimensions | 20 |
| Table 3.8 Compressor First Stage Design Values..... | Error! Bookmark not defined. |
| Table 3.9 HPC Blade Properties | 22 |
| Table 3.10 Compressor Stage 1 Stress..... | 23 |
| Table 4.1 Combustion System Geometry | 27 |
| Table 5.1 Turbine Design Assumptions..... | 29 |
| Table 5.2 Turbine Design Choices..... | Error! Bookmark not defined. |
| Table 5.3 High Pressure Turbine Velocity Triangle Calculations | Error! Bookmark not defined. |
| Table 5.4 Low Pressure Turbine Velocity Triangle Calculations..... | Error! Bookmark not defined. |
| Table 5.5 Turbine Aerothermodynamic Calculations..... | 32 |
| Table 5.6 Turbine Degree of Reaction and Loading Coefficient Calculations..... | 33 |
| Table 5.7 Turbine Blade Design Calculations | 34 |
| Table 5.8 Silicon Carbide Properties | 35 |
| Table 5.9 Turbine Blade Stress Analysis | 36 |
| Table 6.1 Mixer Design Parameters..... | 37 |
| Table 6.2 Mixer Flow Calculations..... | 37 |
| Table 7.1 Nozzle Angles and Sizing..... | 38 |
| Table 7.2 On-Design Nozzle Output Properties | 39 |
| Figure 7.3 Afterburner Geometry | 39 |

Nomenclature

| | | |
|-----------|---|----------------------------------|
| A | = | cross sectional area |
| BPR | = | bypass ratio |
| CMC | = | ceramic matrix composite |
| CO | = | carbon monoxide |
| dB | = | decibel |
| FPR | = | fan pressure ratio |
| g | = | gram |
| GE | = | General Electric |
| h | = | altitude |
| HPC | = | high pressure compressor |
| HPT | = | high pressure turbine |
| kN | = | kilonewton |
| lbf | = | pounds force |
| lbm | = | pounds mass |
| LPT | = | low pressure turbine |
| LTO | = | landing and takeoff |
| M | = | mach number |
| NO_x | = | nitrogen oxide |
| OPR | = | overall pressure ratio |
| P | = | static pressure |
| P_t | = | total pressure |
| RFP | = | request for proposal |
| RPM | = | revolutions per minute |
| RQL | = | Rich-Burn, Quick-Mix, Lean-Burn |
| s | = | second |
| SiC/SiC | = | single crystal silicone carbide |
| SLS | = | sea level static |
| T | = | static temperature |
| T_t | = | total temperature |
| $T_{4.1}$ | = | combustor exit temperature |
| $TSFC$ | = | thrust specific fuel consumption |
| ω | = | rotational speed |
| σ | = | stress |
| π | = | pressure ratio |
| ρ | = | density |

Introduction

This report presents the preliminary design of a candidate engine for a next generation supersonic transport aircraft. The engine, CE18 Bullet, is in response to the RFP [1] which follows the 2006 NASA National Research Announcement calling for a more advanced supersonic airliner. The CE18 Bullet demonstrates significant improvements from the baseline engine found in the NASA N+2 Supersonic Concept study [2] and summarized in the RFP. The figure below shows the proposed 100 passenger supersonic transport aircraft the engine is designed for.

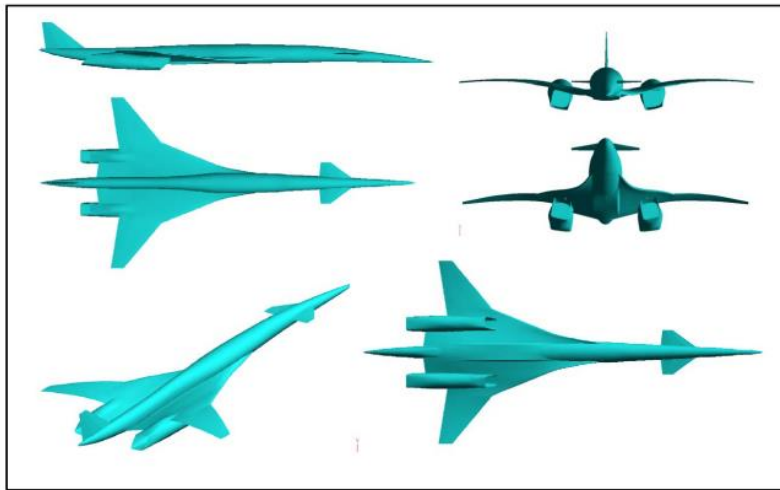


Figure 1.1 NASA N+2 Supersonic Transport Concept

The CE18 Bullet is a mixed-flow turbofan with a design focused on performance improvements from the baseline engine as well as reductions in noise and emissions. Performance improvements of the CE18 Bullet such as fuel consumption and thrust allow the supersonic transport to have a larger operating envelope compared to the baseline engine. Noise and emissions reductions aim to conform to regulatory standards and address issues that have caused prior supersonic transports to be unsuccessful. The engine cycle and component design/analysis was performed using AEDsys engine design software.

1.0 Cycle Analysis

This section details the baseline engine along with the engine cycle selection and overall cycle design of the CE18 Bullet. AEDsys will be validated using the baseline engine information from the RFP then will be used to analyze the CE18 Bullet engine performance both on and off design

1.1 Design Approach

Driving the design of the CE18 Bullet were the performance requirements from the RFP. Requirements were to meet or exceed the baseline engine thrust and to improve upon (lower) the TSFC by at least 5% at four different flight conditions. The flight conditions and minimum performance improvement requirements are shown in the table below.

| Condition | Alt. (ft) | Mach | Temp. | Thrust (lbf) | TSFC (lbm/hr/lbf) | TSFC 5% reduction |
|-------------------|-----------|-------|----------|--------------|-------------------|-------------------|
| SLS | 0 | 0 | std. day | 64625 | 0.520 | 0.494 |
| Takeoff | 0 | 0.25 | hot day | 56570 | 0.652 | 0.619 |
| Transonic Pinch | 40550 | 1.129 | std. day | 14278 | 0.950 | 0.903 |
| Supersonic Cruise | 52500 | 1.6 | std. day | 14685 | 1.091 | 1.036 |

Table 1.1 Baseline Engine Performance Values + 5% reduction in TSFC

Initially, the necessary 5% reduction in TSFC was used as a guide for the engine design with the assumption that improvements in thrust, noise and emissions would occur by default. Upon satisfying the TSFC requirements, further design iterations were aimed at achieving the takeoff thrust and engine design parameters that were realistic at a component level.

1.2 Cycle selection

The given baseline engine was a mixed-flow dual spool turbofan with a relatively low bypass ratio of 1.71. This design is between the high bypass engines on modern commercial transport aircraft and the turbojet engines found on the only two supersonic transport aircraft ever flown, Concorde and Tupolev Tu-144 [3]. Both the Concorde and Tupolev were first flown in the 1960s and have since been retired. In the years since these aircraft, aircraft engine design and technology have progressed to allow for more efficient engine cycles than the turbojet capable of achieving supersonic flight.

The two cycles considered for this study were a mixed flow low-bypass turbofan and a variable cycle. While the variable cycle is a modern and attractive design able to alter bypass ratio for different performance needs, a study by NATO [4] found that a variable cycle achieves its best fuel consumption at the lowest bypass ratio. Considering this along with the complexity of design ruled out the variable cycle. With the baseline engine being a mixed flow low-bypass turbofan and having a better ability to benchmark similar engines of this type, a mixed flow low-bypass cycle was selected for the CE18 Bullet.

1.3 Baseline AEDsys validation

In order to validate the AEDsys engine model software, the baseline engine was modeled using AEDsys and the performance results were compared to the give performance data in the RFP. Primary values for the baseline engine modeled in AEDsys are shown in the table below.

| | | | | | | | | | |
|---|----------------------------|--------|--------|---------|---------|-------------------------|---------------|---------|---------|
| Thrust | 16534 lbf | | | | | Turbomachinery | LP Compressor | 88.32 | |
| Thrust Specific Fuel Consumption | 0.9992 lbm/(hr-lbf) | | | | | Efficiency (%) : | HP Compressor | 85.39 | |
| Bypass Ratio | 1.710 | | | | | | Fan | 89.24 | |
| Thermal Efficiency (%) | 51.79 | | | | | | HP Turbine | 90.80 | |
| Propulsive Efficiency (%) | 75.37 | | | | | | LP Turbine | 91.03 | |
| Station: | 2 | 13 | 2.5 | 3 | 4 | 4.5 | 5 | 8 | 9 |
| Tt (R) | 588.98 | 761.00 | 762.78 | 1746.98 | 3273.00 | 2295.97 | 1906.38 | 1906.38 | 1906.38 |
| Pt (psia) | 5.88 | 13.22 | 13.22 | 205.72 | 195.43 | 39.61 | 16.49 | 12.03 | 11.67 |

Figure 1.2 AEDsys Performance Results for RFP Basline Engine

When thrust and TSFC are compared to values in Table 3 of the RFP for uninstal engine performance, the percent difference in thrust is 0.38% and the percent difference in TSFC is 0.62%. These discrepancies are small enough to be neglected and therefore the AEDsys model is validated.

1.4 New Engine Design

To begin the design of the CE18-Bullet engine, a design point was first determined. The baseline engine was designed at the desired cruise $M = 1.6$ and an $h = 52,500$ feet. As per the RFP, supersonic engines are typically designed for the cruise condition [1]. Because of this, along with a desire to be able to accurately compare the performance of the baseline engine to the CE18 Bullet, the design point was selected as $M = 1.6$ and $h = 52,500$ feet.

Another preliminary step in the engine design was determining suitable efficiencies for each of the major engine components. This was done using the levels of technology efficiencies found in the Aircraft Engine Design text [5]. Given the entry into service date of 2025 from the RFP [1], the component efficiencies were selected as listed in the table below.

| | | | | Polytropic efficiency | | | Overall efficiency | | | |
|----------|-----------|-----------|----------|-----------------------|------------|---------|--------------------|----------------|----------------|-----------|
| Inlet PR | Burner PR | Nozzle PR | Mixer PR | Fan | Compressor | Turbine | Burner | Mech, LP Spool | Mech, HP Spool | Mech, PTO |
| 0.95 | 0.95 | 0.97 | 0.98 | 0.92 | 0.91 | 0.9 | 0.999 | 0.995 | 0.97 | 0.98 |

Table 1.2 CE18-Bullet Component Efficiencies

The next step in designing the overall cycle was to determine the solution space that could satisfy the performance requirements. The solution space was found through an iterative process using carpet

plots which showed the range of TSFC and Specific Thrust values that a given engine design could produce. These carpet plots allowed various different cycle designs to be considered by changing FPR, Combustor Exit Temperature, OPR and Bypass ratio.

1.4.1 On-Design Analysis

With the design point, efficiencies and design approach determined, AEDsys was used to do the iterative carpet plot process. A mixed-flow turbofan, variable specific heat model was used. Using the baseline engine design parameters as starting point for finding the solution space, it was immediately noted that the solution space was very narrow. Even for a wide range of input values, the resulting output ranges of TSFC and Specific Thrust were relatively narrow. In order to analyze the carpet plots and develop performance trends, ranges of the design parameters had to be minimal. Five carpet plots made to determine the solution space and develop trends are shown below.

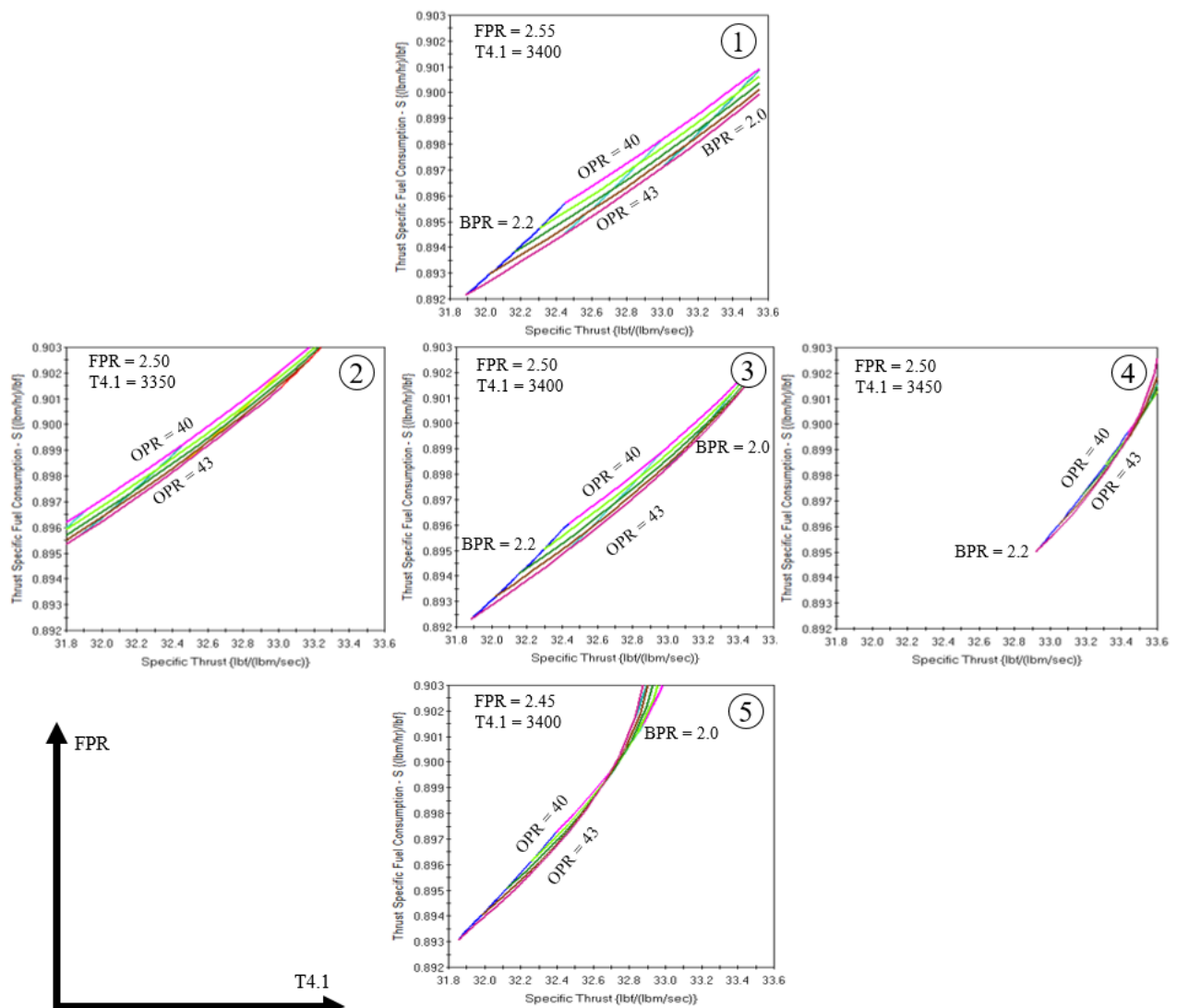


Figure 1.3 Solution Space Carpet Plots for CE18-Bullet

Each of the carpet plots in the figure above has TSFC in terms of (lbm/hr)/lbf on the vertical axis and Specific Thrust in terms of (lbf/(lbm/s)) on the horizontal axis. All five plots use the same scales to effectively identify trends, which results in some plots getting cut off. For reference, each of the five carpet plots entire solution space satisfies the RFP requirement for 5% TSFC improvement at the cruise condition. From the carpet plots, trends relating the design parameters to TSFC and Specific Thrust at the design cruise condition can be determined. General trends are shown in table 1.3.

| Design Parameter | TSFC | Specific Thrust |
|------------------|----------|-----------------|
| Increase FPR | Decrease | Increase |
| Increase T4.1 | Increase | Increase |
| Increase OPR | Decrease | Increase |
| Increase BPR | Decrease | Decrease |

For the given mission, it is desirable to have a low TSFC and a high Specific Thrust. From the trends in table 1.3, carpet plot 1 would contain the lowest

Table 1.3 Design Parameter Performance Trends

TSFC and highest Specific Thrust values. However, considerations do need to be made as to the ability for a component to be designed to meet the overall design parameter value. For example, carpet plot 1 with a FPR of 2.55 could've led to a more complex and heavier fan design. This led to carpet plot 3 from figure 1.3 being selected for the engine cycle parameters. Carpet plot 3, shown in more detail below, also has the largest solution space out of the five carpet plots.

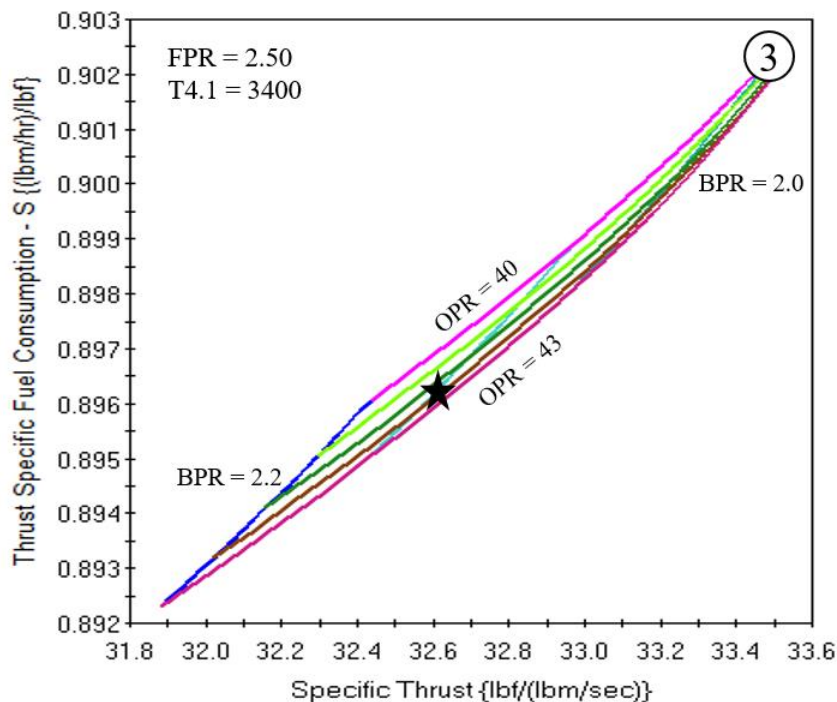


Figure 1.4 Selected Solution Space for CE18-Bullet

The carpet plot in figure 1.4 has a range of OPR and BPR values all at a FPR of 2.50 and T4.1 of 2400. As previously noted, the range of OPR and BPR is relatively narrow. It was found that further increasing the range of these values did not significantly expand the solution space. The solution space in figure # comprises engine cycle designs more advanced than current engines found in the Elements of Propulsion text [6], this was done intentionally and the advanced design of each component will be covered in further sections.

With FPR and T4.1 selected, the carpet plot in figure 1.4 was then used to select OPR and BPR. Because the ranges of TSFC and Specific Thrust varied so slightly, the driving factors for selecting OPR and BPR were practicality of component design and engine weight. OPR of 42 and BPR of 2.1 were selected after iterating through fan/compressor designs. These design values were found to allow for realistic blade heights across the compressor as well as one less compressor stage, reducing engine weight.

Having the four design parameters selected, shown in table 1.4, the final step to complete the engine design was to size it and determine mass flow. With the engine size envelope given in the RFP with a max fan diameter of 89 inches [1], mass flow was determined through an iterative process to ensure adequate thrust at each of the flight conditions previously shown in table 1.1. Having the necessary mass flow of 600 lbm/s, the overall cycle design was complete and the on-design performance was found using AEDsys. The on-design performance results are shown in the figure below.

| Parameter | Value |
|-------------------|-------|
| FPR | 2.50 |
| T4.1 (deg R) | 3400 |
| OPR | 42 |
| BPR | 2.1 |
| Mass Flow (lbm/s) | 600 |

Table 1.4 CE18-Bullet Cycle

| | | | | | | | | | |
|---|----------------------------|--------|--------|---------|---------|-------------------------|---------------|---------|---------|
| Thrust | 19703 lbf | | | | | Turbomachinery | LP Compressor | 89.78 | |
| Thrust Specific Fuel Consumption | 0.8974 lbm/(hr-lbf) | | | | | Efficiency (%) : | HP Compressor | 87.28 | |
| Bypass Ratio | 2.100 | | | | | | Fan | 90.91 | |
| Thermal Efficiency (%) | 57.82 | | | | | | HP Turbine | 91.56 | |
| Propulsive Efficiency (%) | 75.17 | | | | | | LP Turbine | 91.13 | |
| Station: | 2 | 13 | 2.5 | 3 | 4 | 4.5 | 5 | 8 | 9 |
| Tt (R) | 588.98 | 782.63 | 785.06 | 1815.02 | 3400.00 | 2368.49 | 1874.77 | 1874.77 | 1874.77 |
| Pt (psia) | 5.82 | 14.54 | 14.54 | 247.20 | 234.84 | 45.94 | 15.19 | 14.42 | 13.98 |

Figure 1.5 AEDsys On-Design Performance Results for CE-18 Bullet

The above on-design performance values are for the CE18 Bullet a full throttle. However, to accurately compare the CE18 Bullet performance to the baseline engine the throttle was reduced to have the CE18 Bullet thrust match the baseline engine thrust. Reducing the throttle leads to a further drop in TSFC which will be demonstrated in the later section comparing the CE18 Bullet to the baseline engine.

1.4.2 Off-Design Analysis

Similar to the on-design analysis, off-design analysis was done using AEDsys. The on-design reference file for the CE18 Bullet was taken and run at the three other conditions (SLS, Hot-Day Takeoff, Transonic Pinch) provided in the RFP. This allowed the new engine design to be compared against the baseline engine at the four major flight conditions of interest. Results are presented in the next section.

1.5 CE-18 Bullet Performance vs. Baseline Performance

The performance results for the CE18-Bullet are shown in the table below and compared using a percent difference to the baseline engine. This comparison of performance was done using the installed values from the RFP [1]; installation losses required from the RFP were included in the model of the CE18-Bullet. As previously mentioned, the values for TSFC are at a reduced throttle condition due to the CE18-Bullet exceeding the baseline thrust.

| | | Baseline | CE18-Bullet | |
|-------------------|-------------------|----------|-------------|--------|
| | | Value | Value | % Diff |
| SLS | Thrust (lbf) | 64625 | 76985 | 19.1% |
| | TSFC (lbm/hr/lbf) | 0.520 | 0.488 | 6.2% |
| Hot Day Takeoff | Thrust (lbf) | 56570 | 69113 | 22.2% |
| | TSFC (lbm/hr/lbf) | 0.652 | 0.613 | 6.0% |
| Transonic Pinch | Thrust (lbf) | 14278 | 19470 | 36.4% |
| | TSFC (lbm/hr/lbf) | 0.950 | 0.763 | 19.7% |
| Supersonic Cruise | Thrust (lbf) | 14685 | 19703 | 34.2% |
| | TSFC (lbm/hr/lbf) | 1.091 | 0.894 | 18.1% |

Table 1.5 Off-Design Performance Results and Comparison to Baseline

The CE18-Bullet far outperformed the baseline engine thrust at all flight conditions and improved upon the baseline TSFC by over 18% at the transonic pinch and supersonic cruise conditions. TSFC at the SLS condition and Hot Day Takeoff were the only areas where the improvement was near the minimum

of 5%. However, considering the mission of this aircraft the time spent at the hot day condition is minute compared to the time spent at cruise. Therefore, from a fuel burn perspective the great improvement in TSFC at the cruise condition far outweighs the relatively low improvement at takeoff.

The table below shows the thermal and propulsive efficiencies for the CE-18 Bullet at SLS and supersonic cruise. As expected, due to the design point, the best efficiencies were achieved at the cruise condition.

| | SLS | Supersonic Cruise |
|----------------------------|------|-------------------|
| Thermal eff. (%) | 38.4 | 57.8 |
| Propulsive eff. (%) | 1.5 | 75.2 |

Table 1.6 CE18-Bullet Cycle Efficiencies

1.6 Mission and Fuel Burn Analysis

The mission provided by the RFP was for a 100 passenger transport at $M = 1.6$ over a range of 4000 nautical miles [1]. Also provided in the RFP was a detailed climb schedule for the supersonic transport and information for LTO cycle times and throttle settings. This information was used to calculate the fuel required to complete the given mission. Using the provided times from section 2 table 4 of the RFP [1] as well as the calculated values for TSFC in figure 5 above; fuel burn was calculated at LTO. A total time of 6.7 minutes is spent at LTO with 26 minutes spent at idle. Employing a TSFC at takeoff of .613 (lbm/hr/lbf) coupled with the 0.02 hours spent at takeoff and 56570 lbf thrust, a total fuel burn at takeoff was calculated using:

$$Fuel\ Burned = TSFC * Time\ Elapsed * Thrust \text{ (eq. 1.1)}$$

This equation yields a total mass of fuel burned at takeoff of 1719.2 lbm.

Using a similar technique and fuel rates of common transport aircraft at idle [7], the following table was constructed.

| | TSFC (lbm/hr/lbf) | Fuel Mass Flow (lbm/s) | Time Spent | Thrust (lbf) | Fuel Burned (lbm) |
|-----------------------------|-------------------|------------------------|----------------|--------------|-------------------|
| Idle/Taxi | N/A | 1.102 | 1560 Seconds | N/A | 1719.2 |
| Takeoff | 0.613 | N/A | 0.02 Hours | 56570 | 693.5482 |
| Climbout | N/A | 11.023 | 120 Seconds | N/A | 1322.76 |
| Transonic Pinch | 2.586761 | N/A | .0167 Hours | 14278 | 616.794 |
| Cruise | 0.894 | N/A | 4.358558 Hours | 19703 | 57220.85 |
| Descent and Approach | N/A | 1.1 | 210 Seconds | N/A | 231 |
| Total Burn (lbm) | | | | | 61804.1522 |

Table 1.7 Fuel Burn Analysis

The CE18-Bullet burns approximately 82,575 lbm of fuel over the journey, or approximately 11,967 U.S. gallons.

1.7 Other CE18 Bullet Analysis

The following sections provide analyses of the CE18-Bullet less performance metric based and more related to economical and societal impacts of the engine design.

1.7.1 Weight Analysis

Engine weight was determined using benchmark engines. Based on the similar geometry, the General Electric F101 engine provided a suitable base weight model for CE18-Bullet. The diameter to length ratio of the GE F101 is .303 [8] CE18-Bullet has a similar ratio, allowing the engine weight to be approximated based on the F101. The GE F101 has a dry weight of 4,400 lb. Using a linear scale with a size ratio of 2.68:1 for CE18-Bullet to F101, CE18-Bullet's weight reached 11,792 lbs. To scale the weight to modern materials, Cowboy Express multiplied the linearly scaled weight by 0.94 to achieve an engine weight of 11,084 lbs. With these assumptions, the engine is estimated to improve on the 13,000 lb. baseline engine weight by 14.8%.

1.7.2 Noise Analysis

Per the RFP, noise is addressed as an engine exit jet velocity at takeoff. The exit jet velocity of the CE18-Bullet at reduced power takeoff was found to be 1614 ft/s which is above the recommended value of 1375 ft/s. While jet noise calculations are complex and require a variety of different measurements, the increase in velocity of the CE18-Bullet over the recommended value would equate to approximately a 12.8 decibel increase by use of Lighthill's eighth power law [9]. To reduce this increase in noise two different noise attenuation methods will be incorporated into the CE18-Bullet. The first will be an active chevron nozzle, or a chevron excited by piezoelectric actuators, which have been shown to reduce noise up to 12 dB at low frequencies and 4 dB at high frequencies [10]. These chevrons will be incorporated into the nozzle exit similar to the Boeing 787 Dreamliner [11]. The second noise attenuation method will be a helmholtz resonator lining that will help to reduce noise associated with turbomachinery [12].

1.7.3 NOx Analysis

Provided in the RFP were methods of calculating and allowable levels of NOx emissions for the engine design at LTO and cruise conditions. For LTO, the equation shown below [1] gave the allowable NOx emissions of 137.6 g/kN.

$$NOx \text{ Allowable per unit thrust } \left[\frac{g}{kN} \right] = 36 + (2.42 * OPR) \text{ (eq. 1.2)}$$

Using the calculation method specified in the RFP along with data gained from the AEDsys off-design analysis and the ICAO Aircraft Engine Emissions Databank [13] the LTO NOx emissions value for the CE18-Bullet was found to be 215 g/kN. While this value is higher than the allowable value from above, with a modern combustor design and an entry into service of 2025, emissions can be lowered a significant amount [14]

The version of the P₃T₃ method found in [15] was used in calculating the NOx emissions for cruise. The calculated emissions index for the CE18-Bullet was 38 g/kg fuel. This value is significantly higher than the target value of 5 g/kg fuel provided by the RFP [1]. However, the empirical P₃T₃ method may be inaccurate in predicting emissions for a modern engine design such as the CE18Bullet.

1.8 Cycle Design Summary

The overall cycle design of the CE18-Bullet does satisfy the performance requirements of the RFP, but has not been shown to meet the requirements for noise and emissions. The noise and emissions requirements from the RFP are based off values from the N+2 supersonic concept study and are very aggressive even for more efficient and quieter high-bypass turbofans [16].

The next step for the CE18-Bullet was the component design of the inlet, fan/compressor, combustion system, turbine and other intermediate flow sections. The following sections will present the designs of an external compression inlet, a 2-stage fan, a 10-stage compressor, an annular combustor, and a 2-4 stage turbine. All components were made to satisfy the cycle design values of: FPR = 2.5, T4.1 = 3400 R, OPR = 42 and BPR = 2.1.

2.0 Supersonic Inlet Design

The starting point for the design of the candidate engine was the inlet. Supersonic inlets are unique from most commercial engine inlets due to their need to work in both the supersonic and subsonic regime. In order for the inlet to work effectively in a supersonic environment it needs to form a train of oblique shocks to minimize the pressure loss at the terminating normal shock. This is achieved by ramp angles and the use of a 2D inlet face.

2.1 Inlet Type Selection

The inlet is a variable, 2D external compression inlet consisting of two ramps. A 2D geometry was chosen over an axisymmetric inlet because of its ability to change the ramp angles in flight. Two variable ramps were chosen to improve the pressure recovery and to minimize the overall cost due to complexity of manufacturing. External compression was chosen to allow for multiple oblique shock that are external for the system. This allows for a terminating shock to occur at the cowl lip of the inlet. Total pressure recovery is more efficiently conserved through more oblique shocks. However, the gains from having more than two ramps is minute at lower supersonic Mach numbers.

A study from Georgia Tech shows that maximum pressure recovery happens when the oblique shocks are of equal strength [17]. The driving factor for the inlet should be maximum pressure recovery from the free stream flow to the fan [18]. A study by NATO STO from that 1960's shows that cowl lip styled inlets should have a total pressure recovery near 100% at Mach 1.6 [19]. Using the Concorde as a baseline, the inlet type that was selected has shown an already existing application to supersonic transport.

2.2 Inlet Sizing

AEDsys was used to calculate the necessary dimensions of the inlet ramps and lip of the inlet. AEDsys requires a free-stream mach number, the number of desired oblique shocks, and a corrected mass flow to calculate the geometry. The user must specify the angles of any oblique shock ramps, and the software will determine the length of each ramp needed. The goal of designing a supersonic inlet is to keep the total pressure recovery (P_{t2}/P_{t0}) as close to 100% as possible. The ideal situation for this is called

the critical condition, where the oblique shocks generated by the ramps converge to meet the lip of the inlet with no spillage. Spillage flow induces extra drag on the engine as well as subcritical and supercritical conditions decrease the pressure recovery, however supercritical has a much more severe impact on the inlet pressure recovery.

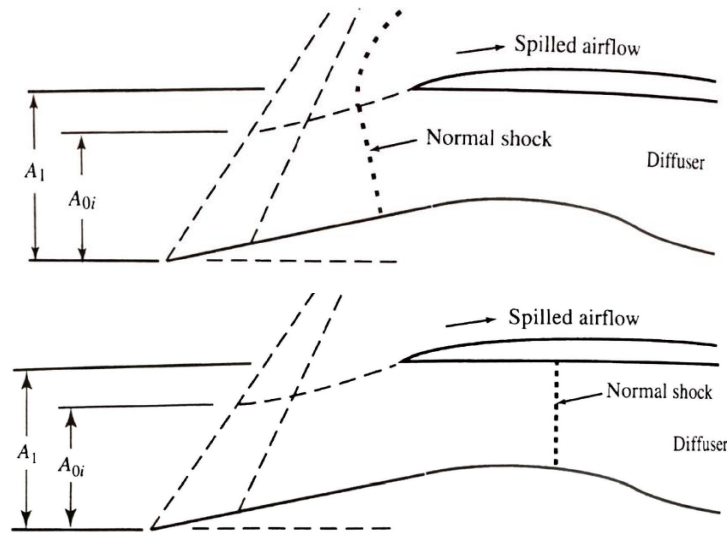


Figure 2.1 Subcritical inlet operation [5]

To decide the ramp angles for the least amount of total pressure loss, AEDsys provides a contour plot. Figure 2.2 is a colored contour plot at the cruise flight condition of $M = 1.6$. Increasing the ramp angle too much creates a strong oblique shock, resulting in a loss of total pressure. This is represented by the upper right corner of figure 2.2. Therefore, the ideal solution is always to have both ramp angles be equal to turn the flow as gently as possible. As seen in Figure 2.2, there is an island of peak pressure recovery with many possible solutions.

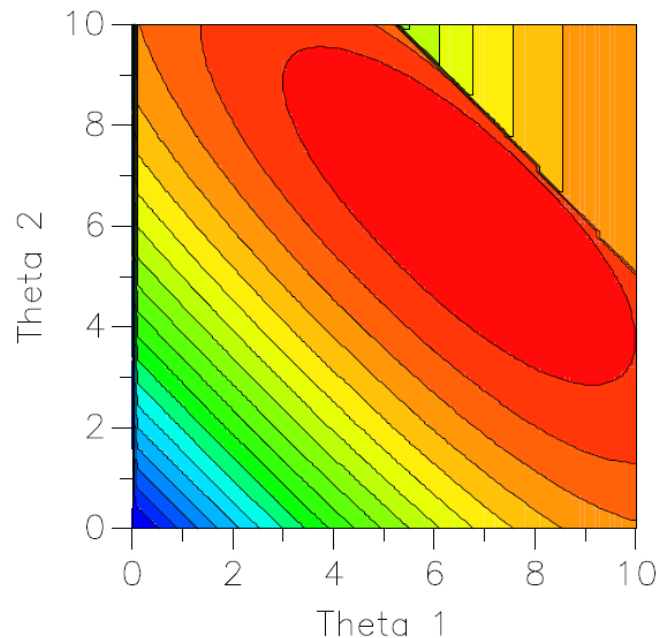


Figure 2.2 Pressure Recovery with Varying Inlet Angles at Cruise Condition

However, it is desired to increase the ramp angle as much as possible while still maintaining high pressure recovery to save weight and to reduce the overall length of the engine. To achieve this, the ramp angles were chosen to be seven degrees.

The figure below shows the geometry of the inlet at the on-design critical condition. This geometry was produced by AEDsys and shows both the oblique shocks and the terminating normal shock. The on-design performance values for this inlet are listed in table 2.1.

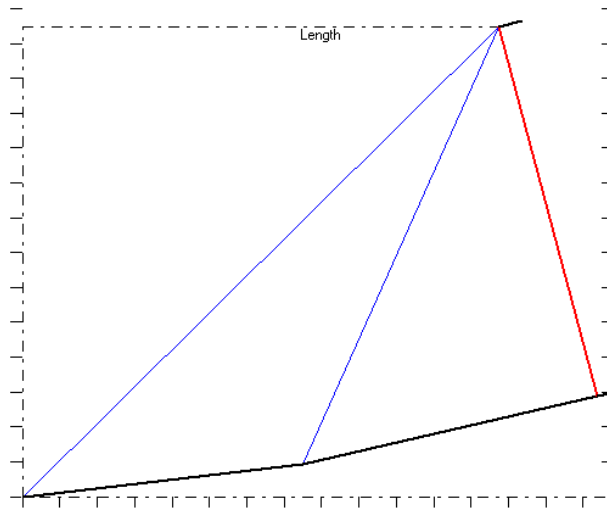


Figure 2.3 Supersonic Inlet Geometry

| Parameter | P_{t2}/P_{t0} | M_2 | P_2/P_0 | A_2/A_0 | A_0 (ft ²) | \dot{m}_{corr} (lbm/s) |
|--------------|-----------------|-------|-----------|-----------|--------------------------|--------------------------|
| Value | 0.990 | 0.941 | 2.378 | 0.810 | 45.5 | 1797.0 |

Table 2.1 Inlet On-Design Performance Values

2.3 Inlet Off-Design Performance

Because the same ramp configuration for cruise condition will not provide critical inlet operation for other legs of the mission, the ramp angles must be scheduled according to the flight Mach number. Optimizing the ramp angles for each flight condition to minimize total pressure loss yields the following, where the “Milspec” curve is based on the equation [5]:

$$\eta_{R \text{ spec}} = 1 - 0.075(M_0 - 1)^{1.35} \quad (\text{eq. 2.1})$$

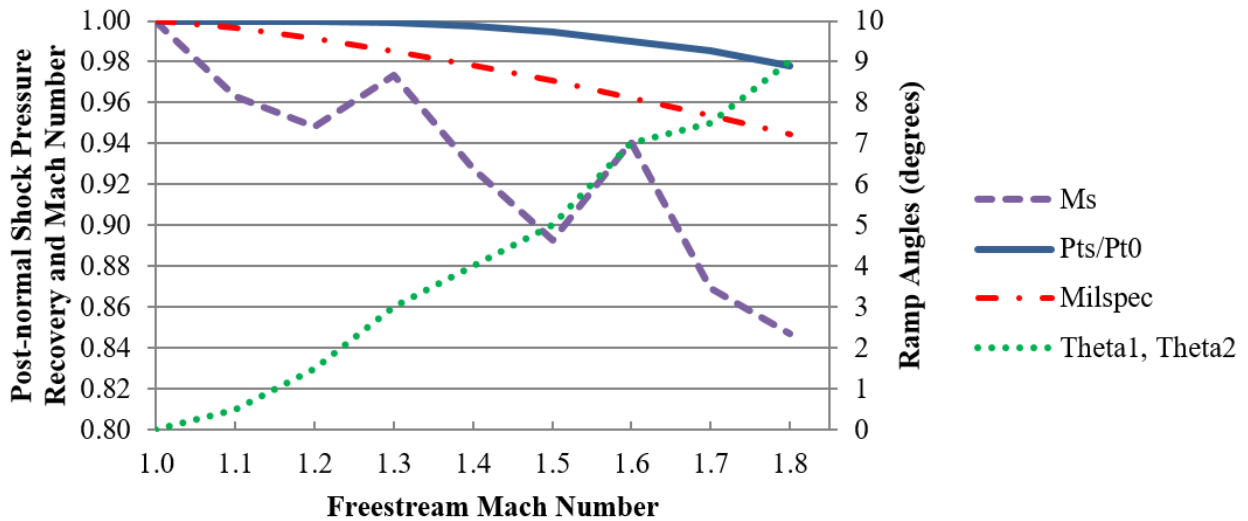


Figure 2.4 Off-Design Inlet Performance with Ramp Scheduling

It can be seen that by carefully changing the inlet ramp angles, the Milspec curve can be surpassed by a significant percentage. At cruise, the designed inlet incurs almost three times less total pressure loss.

2.4 Inlet Bleed Flow

In supersonic flight, the air captured by the inlet is a product of the capture area and the flight speed. Therefore, it is not necessarily true that the air brought in by the inlet is capable of being ingested by the engine. In this case, it is required that some of the flow be bled to the ambient air. This is done by opening a small ramp to guide a portion of the air outside which can be opened and closed as flight conditions and the required mass flow from the engine change.

2.5 Inlet Diffuser

The front section of the inlet has a rectangular, “2D,” cross-section; however, the engine has a circular, or “annular,” section. Therefore, there must be a transition between these two shapes. To achieve this, a diffuser section must be added. It is important for a diffuser to not add any unnecessary vortices to the flow so as to decrease the cyclic stresses on the fan blades, resulting in a longer fatigue life. The double angle of the diffuser section is approximately five degrees and the length to width ratio is roughly two. For purely circular diffusers, this would be very conservative. However, due to vortices potentially being generated by corners during the cross section transition, the diffuser was given additional length.

2.6 Inlet Drag

Following the guidelines set out in the RFP, the inlet drag was calculated to be approximately 4.3% of the thrust produced. According to the RFP if the inlet is properly designed the spillage and bypass drag should be 0. The candidate engines inlet produces no bypass or spillage drag, showing that it is properly designed. The drag produced by the inlet is all accounted for by bleed drag.

2.7 Inlet Model

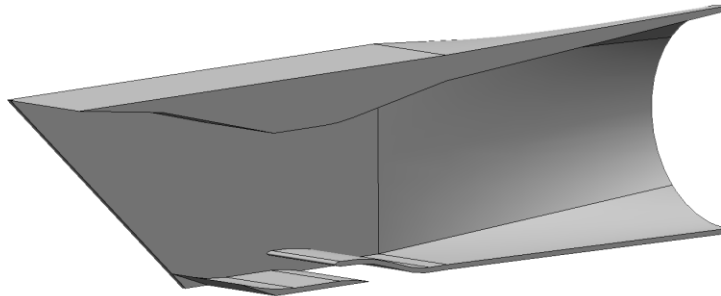


Figure 2.5 Supersonic Inlet CAD Model

3.0 Fan and Compressor Design

From the request for proposal, the baseline engine was a mixed-flow turbofan. The fan pressure ratio was 2.25 using 2 stages and the compressor had 11 stages for an overall pressure ratio of 35. From this starting point and the overall cycle requirements outlined in section 1 above, a new fan and compressor were designed. The following section will detail the design of a 2-stage fan and a 10-stage compressor for the CE18-Bullet.

The design process started with the necessary OPR then determining necessary amount of stages and angular velocity of the two spools. The fan will operate on the low-speed spool and the HPC will operate on the high-speed spool. Assuming a free-vortex allowed velocity profiles across the whole compression system to be determined. The velocity profiles shown across a rotor and stator in figure 3.1 utilize velocity triangles to show flow characteristics across a blade's hub, pitchline, and tip stream surfaces.

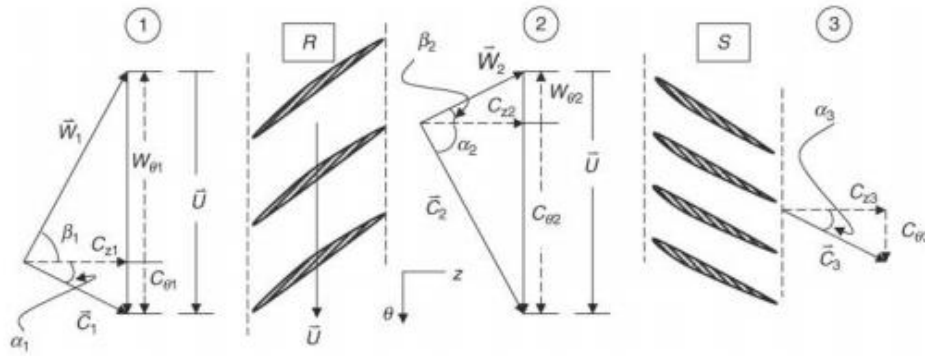


Figure 3.1 Fan/Compressor Velocity Triangle Nomenclature [20]

In order to check the design parameters of the fan and compressor blades and ensure realistic values, the following table of acceptable ranges will be used.

| Parameter | Range of Values | Typical Value |
|--------------------------------------|----------------------------------|---------------|
| Flow Coefficient, ϕ | $0.3 \leq \phi \leq 0.9$ | 0.6 |
| D-Factor | $D \leq 0.6$ | 0.45 |
| Axial Mach Number M_z | $0.3 \leq M_z \leq 0.6$ | 0.55 |
| Tip Tangential Mach Number M_T | 1.0-1.5 | 1.3 |
| Degree of Reaction | $0.1 \leq \circ R \leq 0.90$ | 0.5 |
| Tip Relative Mach Number (1st Rotor) | $(M_{1r})_{tip} \leq 1.7$ | 1.3-1.5 |
| Stage Average Solidity | $1.0 \leq \sigma \leq 2.0$ | 1.4 |
| Stage Average Aspect Ratio | $1.0 \leq AR \leq 4.0$ | <2.0 |
| Polytropic Efficiency | $0.85 \leq e_c \leq 0.92$ | 0.9 |
| Loading Coefficient ψ | $0.2 \leq \psi \leq 0.5$ | 0.35 |
| NACA-65 series (range) | $M \leq 0.8$ | <0.8 |
| De Haller criterion | $V_{2R} \sqrt{V_{1R}} \geq 0.72$ | 0.75 |
| Taper Ratio | $\sim 0.8-1.0$ | 0.8 |

Table 3.1 Guidelines on Range of Compressor Parameters [20]

3.1.0 Fan

The CE-Bullet is a low bypass turbofan engine. The fan operates with a bypass ratio of 2.1 with a total air mass flow after bleed being 600.3 lbm/s. From the mission analysis, the fan needed to achieve a pressure ratio of 2.5 at cruise. In design, a pressure ratio of 2.48 was achieved. It was impractical to continue iterating to more decimal places on values such as solidity, diffusion, and incoming flow angle because it makes the manufacturability increasingly difficult. To make up for the deficit the compressor was designed to have a higher pressure ratio than what was necessary to compensate. The spool that the fan connects to the low-pressure turbine spins at a rate of 4422 RPM. The fan was assumed to have a

diameter of 89 inches, the size envelope for the engine. This size was used to drive the fan design. Table 3.2 below gives the fan design parameters and parameters used for IGV to prepare the flow for ingestion into the fan.

| Design Parameter | Value | Design Parameter | Value |
|---------------------|-------|------------------|-------------|
| π | 2.48 | Rotational Speed | 4422 RPM |
| e | .91 | σ_{IGV} | 0.8 |
| α_0 | 0 | IGV Loss Coeff. | 0.02 |
| M_0 | 0.5 | IGV chord/height | 0.5 |
| Stator Loss Coeff. | 0.02 | Number of Stages | 2 |
| Rotor chord/height | 0.5 | Mass Flow Rate | 600.3 lbm/s |
| Stator chord/height | 0.5 | σ | 1.12 |
| P_{t2} | 6.002 | T_{t2} | 589.6 R |
| M_1 | 0.6 | α_1 | 22 |

Table 3.2 Fan and Inlet Guide Vane

3.1.1 Inlet Guide Vane

The fan utilizes a set of inlet guide vanes (IGV) to introduce a flow swirl angle into the first rotor. Increasing the swirl angle gives a higher total temperature per stage, which increases the overall pressure ratio. This gives the fan the ability to take part of the load off the compressor by having a higher fan pressure ratio. There is the ability that if the IGV were to choke the flow it can create a sonic barrier, which can reduce the amount of fan noise created [21]. Additionally, designing a variable guide vane allows finer control of the inlet swirl angle allowing the fan to have the optimum flow angle at different off design conditions.

3.1.2 Fan Stage and Blade Design

Once all the required design decisions were determined, the fan stage-by-stage calculations were calculated using AEDsys COMPR. Calculations for the first stage were first performed by hand. Due to the repetitive nature of going through multiple stages. AEDsys aids in the design by automatically do the addition stage calculations. Table 3.3 below contains the velocity triangle and aerothermodynamic calculations for the first stage of the fan.

The stations in the table above are in order are before in rotor, after the rotor and before the stator, then after the stator. These values come after the inlet guide vane has introduced swirl increasing the overall pressure ratio that the fan produces.

| Parameter | Station 1 | | | Station 2 | | | Station 3 | | |
|-------------|-----------|--------|--------|-----------|--------|-------|-----------|--------|--------|
| | Hub | Mean | Tip | Hub | Mean | Tip | Hub | Mean | Tip |
| U (ft/s) | 416.3 | 1067.6 | 1718.9 | 520.9 | 1067.6 | 1615 | 613.8 | 1067.6 | 1521.3 |
| u (ft/s) | 639.5 | 639.5 | 639.5 | 639.5 | 639.5 | 639.5 | 639.5 | 639.5 | 639.5 |
| Vel (ft/s) | 920.9 | 689.7 | 659.3 | 1779.1 | 1031.7 | 834.0 | 781.6 | 689.7 | 664.7 |
| v (ft/s) | 662.6 | 258.4 | 160.5 | 1149.9 | 887.3 | 722.3 | 384.6 | 310.1 | 259.8 |
| α | 46.02 | 22.00 | 14.09 | 68.93 | 51.7 | 39.93 | 35.09 | 22 | 15.83 |
| β | - | -51.7 | - | - | -22 | - | - | -51.7 | - |
| M_{abs} | .825 | .600 | .572 | 1.762 | .86 | .678 | .632 | .553 | .532 |
| r (in) | 10.79 | 27.67 | 44.55 | 13.5 | 27.67 | 41.85 | 15.91 | 27.67 | 39.43 |
| T (R) | 519 | 550 | 553.4 | 424.1 | 599.0 | 629.7 | 636.8 | 648.0 | 650.8 |
| T_t (R) | 589.6 | 589.6 | 589.6 | 687.6 | 687.6 | 687.6 | 687.6 | 687.6 | 687.6 |
| P (psi) | 3.83 | 4.69 | 4.79 | 1.82 | 6.08 | 7.25 | 7.46 | 7.93 | 8.06 |
| P_t (psi) | 5.98 | 5.98 | 5.98 | 9.86 | 9.86 | 9.86 | 9.76 | 9.76 | 9.76 |

Table 3.3 Fan Velocity Triangle and Aerothermodynamic Calculations

After calculating the thermodynamic properties across the fan stages, the geometric dimensions were then determined. The table below gives the dimensions for the flow path of the fan.

| Station | Hub Radius (in) | Tip Radius (in) | Area (in ²) |
|------------------|-----------------|-----------------|-------------------------|
| Inlet Guide Vane | 10.08 | 45.27 | 6118.7 |
| Fan Inlet | 10.79 | 44.55 | 5870.7 |
| Fan Exit | 19.05 | 36.3 | 2999.04 |

Table 3.4 Fan Geometry

The length of the fan is 75 inches, which is to be expected with a fan of this size. The first set of rotor blades are close to 30 inches and the last stator blades are close 17 inches long.

Ultimately, the fan resulted with a stage loading coefficient of 0.5161 and flow coefficient of 0.5988. The rotor becomes supersonic towards the tip, which can be expected with some fan designs. To prevent the blades from stalling the fan incorporates blade twist throughout the span. As shown in the figure below is the first stage of the fan rotor on the left and stator on the right. The blue region is the blades at 25% of the span of the blade.

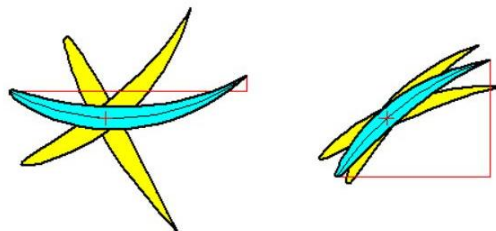


Figure 3.2 Fan Airfoil and Twist

3.1.3 Fan Model

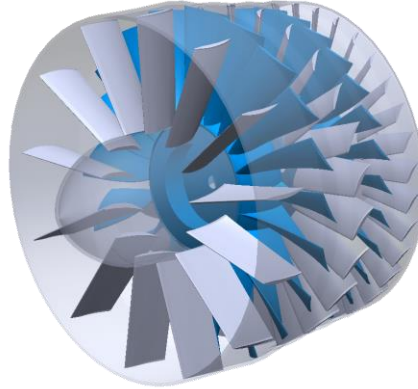


Figure 3.3 Fan CAD Model

3.2.0 High Pressure Compressor

With the desired overall pressure ratio of 42 and an achieved FPR of 2.48, the required high-pressure compressor (HPC) pressure ratio needed to be approximately 17.1. To handle the required loading the HPC has 10 compression stages with an inlet guide vane operating at 8,116 RPM, and a polytropic efficiency of 0.9 across the whole section. HPC design choices, requirements, and inlet properties are as shown below in table 3.5.

| Design Parameter | Value | Design Parameter | Value |
|---------------------|-------|------------------------|--------|
| π_{HPC} | 17.1 | Rotational Speed (RPM) | 8116 |
| e_{HPC} | 0.9 | σ_{IGV} | 0.9 |
| α_0 | 0 | IGV Loss Coeff. | 0.03 |
| M_0 | 0.5 | IGV chord/height | 0.6 |
| Stator Loss Coeff. | 0.03 | Number of Stages | 10 |
| Rotor chord/height | 0.5 | Mass Flow Rate (lbm/s) | 193.64 |
| Stator chord/height | 0.5 | σ_{HPC} | 1.29 |
| $P_{t2.5}$ (psi) | 14.86 | $T_{t2.5}$ (R) | 785.6 |
| M_1 | 0.55 | α_1 | 25 |

Table 3.5 Compressor and Inlet Guide Vane Parameters

As seen in table 3.5, the inlet guide vane has incoming flow at 0 degrees at a Mach of 0.5 to turn the flow 25 degrees into the first rotor. An average stage solidity of 1.29 was selected for the high pressure compressor, which is within the acceptable range of values in table 3.1.

The input properties from above are capable of being plugged into COMPR, an AEDsys subprogram, and through multiple manual iterations the HPC dimensions were determined. The COMPR program's validity was checked through hand calculations, and all parameter's calculations matched up.

3.2.1 HPC Stage Design

Once the iterations in COMPR had been completed, a detailed design of the compressor was completed. A free vortex swirl distribution assumes axial velocity and total enthalpy do not vary with radius, and through the Euler pump equation a constant-work compressor was assumed [5]. Applying a free vortex swirl distribution the compressor components and velocity triangles were created. Velocity triangles were calculated for the hub, mean, and tip of all HPC stages [20]. The values for the HPC first stage velocity triangles are shown in table 3.6, with front and back end annulus dimensions shown in table 3.7.

| Parameter | Stage 1 | | | Stage 2 | | | Stage 3 | | |
|-------------------|---------|---------|---------|---------|---------|---------|---------|---------|---------|
| | Hub | Mean | Tip | Hub | Mean | Tip | Hub | Mean | Tip |
| U (ft/s) | 880.5 | 1197.1 | 1514.4 | 923.67 | 1197.08 | 1471 | 965.36 | 1197.1 | 1429.42 |
| C_z (ft/s) | 665 | 665 | 665 | 665 | 665 | 665 | 665 | 665 | 665 |
| C (ft/s) | 787.5 | 733.8 | 708.8 | 1328.4 | 1108.8 | 981.8 | 768.2 | 733.8 | 714 |
| C_θ (ft/s) | 421.8 | 310.1 | 245.2 | 1149.9 | 887.3 | 722.3 | 384.6 | 310.1 | 259.8 |
| W (ft/s) | 807.83 | 1108.80 | 1432.88 | 702.43 | 733.80 | 1001.01 | 882.96 | 1108.59 | 1345.45 |
| W_θ (ft/s) | 458.66 | 887.30 | 1269.22 | -226.23 | 310.10 | 748.20 | 580.86 | 886.98 | 1169.62 |
| α | 32.39 | 25 | 20.24 | 59.96 | 53.15 | 47.36 | 30.04 | 25 | 21.34 |
| β | 59.96 | 53.15 | 47.36 | 32.39 | 25 | 20.24 | 59.96 | 53.15 | 47.36 |
| M_{abs} | 0.593 | 0.55 | 0.53 | 0.987 | 0.801 | 0.699 | 0.537 | 0.512 | 0.497 |
| M_{rel} | 0.608 | 0.831 | 1.071 | 0.522 | 0.530 | 0.713 | 0.617 | 0.773 | 0.937 |
| r (in) | 12.43 | 16.904 | 21.38 | 13.04 | 16.904 | 20.76 | 13.63 | 16.9 | 20.18 |
| T (R) | 734 | 740.8 | 743.8 | 753.8 | 798.3 | 820.4 | 851.5 | 855.8 | 858.2 |
| T_t (R) | 785.6 | 785.6 | 785.6 | 900.7 | 900.7 | 900.7 | 900.7 | 900.7 | 900.7 |
| P (psi) | 11.71 | 12.1 | 12.27 | 12.37 | 15.12 | 16.63 | 18.78 | 19.12 | 19.3 |
| Pt (psi) | 14.86 | 14.86 | 14.86 | 23.06 | 23.06 | 23.06 | 22.86 | 22.86 | 22.86 |

Table 3.6 Compressor Velocity Triangle and Aerothermodynamic Calculations

| Station | Hub Radius (in) | Tip Radius (in) | Area (in ²) |
|------------------|-----------------|-----------------|-------------------------|
| Inlet Guide Vane | 12.59 | 21.22 | 915.89 |
| Compressor Inlet | 12.43 | 21.38 | 951 |
| Compressor Exit | 16.31 | 17.49 | 125.3 |

Table 3.7 Compressor Dimensions

| Parameters | Rotor | | | Stator | | |
|--------------------|-------|-------|-------|--------|-------|-------|
| | Hub | Mean | Tip | Hub | Mean | Tip |
| Diffusion Factor | 0.372 | 0.540 | 0.479 | 0.594 | 0.540 | 0.497 |
| ψ | 0.463 | 0.482 | 0.493 | - | - | - |
| ϕ | 0.423 | 0.555 | 0.687 | 0.433 | 0.555 | 0.677 |
| De Haller | 0.870 | 0.662 | 0.699 | 1.257 | 1.511 | 1.344 |
| $^{\circ}R$ | 0.149 | 0.500 | 0.671 | 0.205 | 0.500 | 0.656 |
| $P_{t,exit}$ (psi) | - | - | - | 254.7 | 254.7 | 254.7 |
| $T_{t,exit}$ (R) | - | - | - | 1936 | 1936 | 1936 |
| $M_{abs,exit}$ | - | - | - | 0.347 | 0.344 | 0.342 |

Table 3.8 Compressor First Stage Design Values

The HPC ended up with a pressure ratio of 17.1, meeting the necessary value from above. Exit properties are as seen in table 3.8 as well as all resulting parameters, which are within their acceptable ranges in reference to 3.1.

3.2.2 HPC Blade Design

To determine the best cascade(s) for the HPC the mach numbers of the flow across each stage were used. Because all stages have subsonic flow except for one, NACA 65-series airfoils were selected for the entirety of all blades except stage 1 [20]. Stage 1 has transonic flow towards the tip, therefore it has a NACA 65-series airfoil at the hub while transitioning to a controlled diffusion airfoil at the tip. A controlled diffusion airfoil was selected for the tip of stage 1 because they are designed to be shock-free at transonic mach numbers [22]. To obtain optimal performance across all stages it is necessary to calculate the optimal incidence and deviation angles through multiple iterations, and therefore a desirable NACA 65-series airfoil [20]. The process is as outlined in figure 3.4.

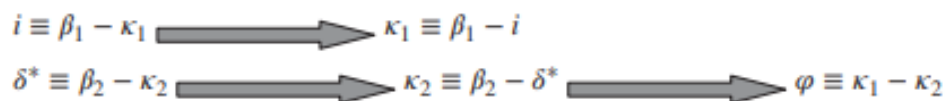


Figure 3.4 Blade Incidence and Deviation Angles [20]

The COMPR subprogram provides the optimal incidence and deviation angles across all HPC rotors and stators. COMPR superimposes an airfoil onto each stage and shows the twist required throughout the blade's span to prevent stalling. Figure 3.5 shows the first stage's rotor and stator twist, with the blue cascade being at 50% radius and the yellow cascade designating the hub and tip twists. General blade properties for the HPC are given in table 3.9.

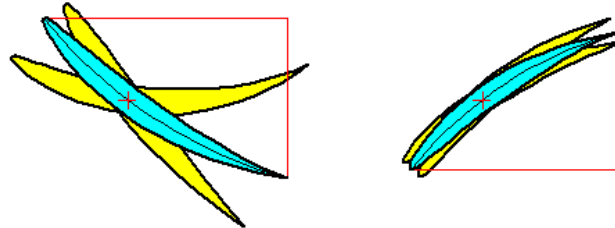


Figure 3.5 Compressor Airfoil and Twist

| Parameter | Rotor | Stator |
|--------------------------|--------|--------|
| Hub to Tip Ratio | 0.6 | 0.65 |
| Mean Radius (in) | 16.904 | 16.904 |
| Number of Blades | 34 | 39 |
| Aspect Ratio | 2 | 2 |
| Taper Ratio | 0.8 | 0.8 |
| Stagger Angle (deg) | 42 | 42 |
| Stage 1 Blade Chord (in) | 4.17 | 3.57 |
| σ | 1.29 | 1.29 |
| Spacing | 3.12 | 2.72 |

Table 3.9 HPC Blade Properties

Another large component implemented in the HPC design is variable stator vanes. While the engine is off design the variable stator vanes prevent choking, stall, and compressor surges by optimizing flow angles. These variable vanes are implemented in 4 different sections as similar to current technology: IGV, stages 1-3, stages 4-7, and 8-11 to optimize performance across all stages [23].

3.2.3 HPC Structural Analysis

The HPC will be made with SiC/SiC CMC, whose properties are $\rho=0.0758\text{lb/in}^3$ and $\sigma_{\text{all}}=38000\text{psi}$ [24]. The blades in the compressor will need to be able to withstand multiple different

stresses. The compressor has a high angular velocity causing a large centrifugal stress, plus it will need to withstand a total temperature of 1936 R at the exit of the compressor and high frequency vibrations throughout. The most important stress of these is centrifugal stress on the blade [5], the centrifugal stress on a blade was calculated using the equation below. Table 3.10 shows the data necessary to calculate the centrifugal stress at the stage 1 rotor of the HPC and the compressor stage's margin of safety.

$$\sigma_c = \frac{\rho \omega^2 A}{4\pi} \left(1 + \frac{A_t}{A_h} \right) \text{ (eq. 3.1)}$$

| Parameter | Value |
|------------------|---------------------------|
| ρ | 0.0753 lb/in ³ |
| ω | 8,116 RPM |
| A | 951 in ² |
| A_t/A_h | 0.8 |
| σ_c | 19320psi |
| σ_{all} | 38000psi |
| Margin of Safety | 0.961 |

Table 3.10 Compressor Stage 1 Stress

3.2.4 HPC Overall

Overall, the CE-18 high-pressure compressor is 43.89 inches long. With Sic/Sic CMC weight of the HPC is saved while still having a margin of safety of 0.961 on centrifugal stress. The HPC also has 10 compression stages instead of the baseline engine's 11 stages. All required values (e.g. diffusion factor, solidity, flow coefficient, and stage loading) are within the typical range of values as provided by table 3.1. The multi-section variable stator vanes allow for a large HPC operation envelope helping prevent choking, stall, and compressor surges.

3.2.5 Compressor Model

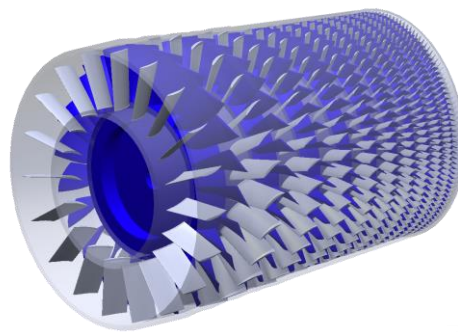


Figure 3.6 Compressor CAD Model

4.0 Combustion System Design

The following subsections address the design and analysis of the combustion system implemented in the CE18-Bullet. Described throughout are the designs of the combustor pre-diffuser and combustor geometries. Also addressed is the selection of: emission control and cooling techniques, fuel injection methods, and materials.

Per the RFP and engine cycle analysis the burner must achieve: low NO_x emissions, high burner efficiency, a T4.1 of 3400 R, and a P4.1 of 210 psi, all while maintaining the high performance requirements of a supersonic transport aircraft. In order to achieve these performance requirements and design values, a Rich-Burn, Quick-Mix, Lean-Burn (RQL) combustor was selected. The logic behind this selection and specifics of an RQL combustor are discussed in detail in section 4.2. The combustor was designed at the maximum dynamic pressure condition as this establishes both the maximum gas temperature and maximum throughout condition [5]. From the flight profile provided in the RFP, and max velocity chosen by the team, the maximum dynamic pressure condition occurs during the climbing cruise at an altitude of 52,500 Ft and Mach 1.8.

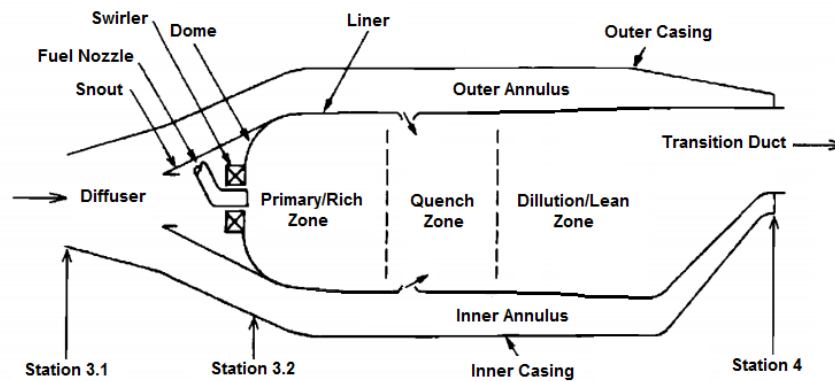


Figure 4.1 RQL combustor [5]

The figure above was adapted to show the typical principal features and components of an RQL combustor.

4.1 Diffuser Design

Air exits the compressor and enters station 3.1 shown above at Mach 0.29 and must be slowed to Mach 0.08 in order to insure proper combustion of the fuel. To achieve this velocity drop between the diffuser entrance and exit the burner uses a flat wall and dump diffuser. The flat wall diffuser has 2 equally spaced splitter veins with 2Θ at 9° as is desired according to the Mattingly text [5]. This text also states that increasing the number of splitter veins allows for a shorter diffuser. However, Mattingly goes on to state that the geometric complexity and difficulty of manufacturing sets the practical limit of splitter veins at 2 [5]. Figure 4.2 shows the effect of introducing a splitter vein on the overall length of the diffuser.

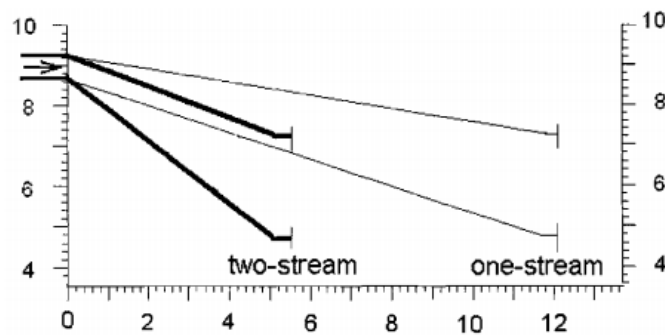


Figure 4.2 Effect of Splitter Veins

4.2 Rich Burn – Quick Mix – Lean Burn (RQL)

The RQL configuration was developed in response to the growing need to reduce pollutant emissions in gas turbine engines. In the application of high altitude and speed transportation this need is multiplied due to the risk NO_x emissions has on the depletion of ozone in the stratosphere where the aircraft will fly [25]. In a RQL combustor the primary zone equivalence ratio is above unity, fuel-rich. Operating at a fuel-rich condition has been shown to be a more stable combustion than operating at a fuel-lean and allows for the temperature in the primary zone to be suppressed. The reduction in temperature and lack of oxygen in the primary zone results in less NO_x being produced. The mixture exiting the primary zone is still highly concentrated in energetic hydrogen and hydrocarbon radicals that must be burned or oxidized. Air that circumvented the primary zone is now introduced through wall jets and mixed to create a lean-burn condition to process the reactants. If conditions are met the emissions leaving the combustor should be relatively clean with little pollutants [26]. Based on this method and additional research on typical RQL combustors a primary zone equivalence ratio Φ_{PZ} of 1.6 was selected.

4.3 Materials and Cooling Methods

According to the Mattingly text, the material with the highest oxidation resistance is Hastelloy X [5]. Hastelloy X is a nickel-based super alloy which has a useful temperature of 2200° R which was prominent in industry from the 1960's to 1980's [27]. However, due to the need to keep a fuel rich mixture in an RQL system, cooling flow cannot be introduced into the primary zone [26]. This creates a major challenge in selecting a liner material to withstand the high temperatures. For this reason, more advanced materials such as ceramic matrix composites (CMC's) with environmental barrier coatings will be required for the CE18. According to NASA, a CMC combustor equipped with an EBC can achieve temperature capabilities upwards of 3000° R which lowers cooling flow requirements and NO_x emissions while increasing combustion efficiency [28]. While transpiration/effusion cooling can provide more cooling with the same amount of cooling flow when compared to convection/film cooling, it presents additional design problems including manufacturing and sustainability. Transpiration/effusion cooled combustors often face clogging problems from internal oxidation and particles and have decreased strength due to their porous state [29]. In order to limit the required maintenance on the engine, a conventional film cooled liner was selected. Figure 4.3 below shows cooling effectiveness values of transpiration vs film cooling over a range of air flow fraction values.

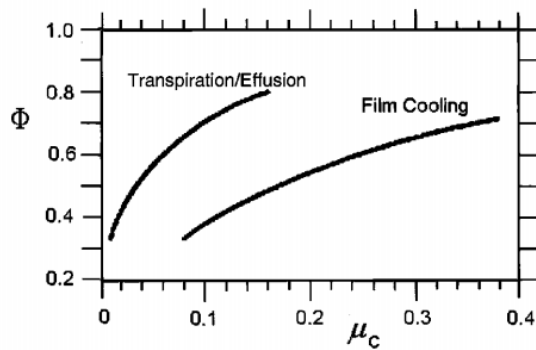


Figure 4.3 Cooling Effectiveness

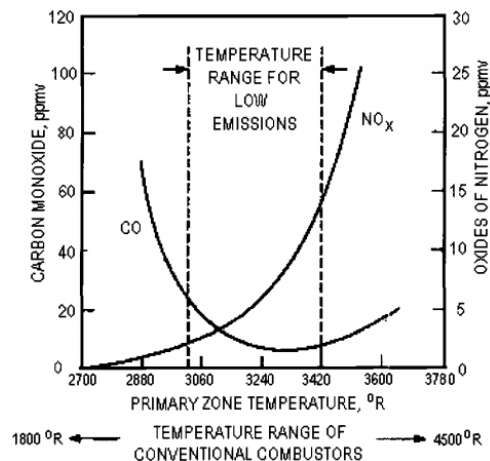


Figure 4.4 CO and NO_x Emissions

Figure 4.4 above from the Mattingly text shows CO and NOx emissions at various primary zone temperatures. Based on this diagram a gas temperature of 3240° R was selected in order to achieve the lowest emission levels.

4.4 Combustor Geometry

The combustor geometries were calculated using the AEDsys software package MAINBURN which were imported into the CAD software to create the 3D images provided at the end of this section. The total length of the combustor was found to be approximately 30 in. Additional geometric values calculated for each section of the combustor and number of swirlers are provided in table below.

| L_{diff} | L_{pz} | L_{sz} | L_{nozzle} | L_{total} | $N_{swirlers}$ |
|------------|----------|----------|--------------|-------------|----------------|
| 9.4 in | 2.2 in | 11.5 in | 6.8 in | 29.9 in | 16 |

Table 4.1 Combustion System Geometry

4.5 Fuel Injection Technique & Ignition Source

The CE18-Bullet will utilize standard air-blast atomizers and surface discharge igniters due to their known reliability and history of use in industry. Air blast atomizers produce a fine mist of fuel to ensure proper mixing with the air which increases efficiency and decreased pollutants and smoke from the engine.

4.6 Combustor Model

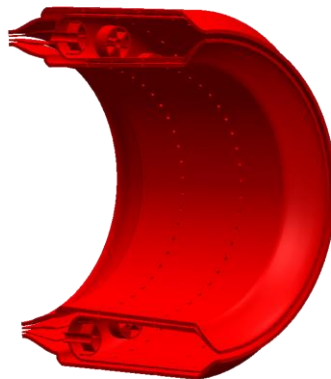


Figure 4.5 Annular Combustor CAD Model

5.0 Turbine Design

The turbine's primary purpose is to extract power from the energized flow leaving the combustor such as is sufficient to power the compressor and fan to achieve the necessary pressure gain. The CE18-Bullet is a dual spool design, meaning it contains a high pressure turbine (HPT) on the same mechanical shaft as the high pressure compressor, and a low pressure turbine (LPT) on the same mechanical shaft as the fan. Multiple designs were considered, however it was determined that a design consisting of a 2 stage LPT and a 2 stage HPT was optimal. The following section will discuss the analysis necessary to complete a component level design of the CE18-Bullet turbine. For velocity triangle calculations, nomenclature in the figure below will be used.

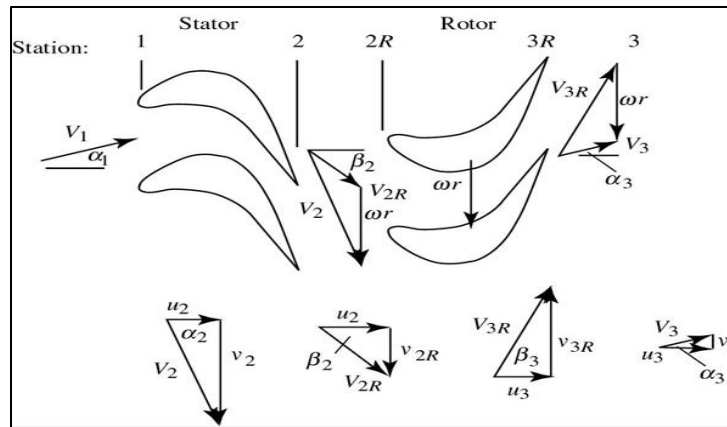


Figure 5.1 Turbine Velocity Triangle Nomenclature

5.1 Turbine Design Analysis and Approach

The design process began with a first law reverse power balance between hot and cold section turbomachinery using equations 5.1 and 5.2.

$$\dot{m}_{core} c_{pt} (T_{t4} - T_{t4.5}) = \dot{m}_{core} c_{pc} (T_{t3} - T_{t2.5}) \eta_{mech} \quad (\text{eq. 5.1})$$

$$\dot{m}_{core} c_{pc} (T_{t2.5} - T_{t2}) = \dot{m}_{core} c_{pt} (T_{t4.5} - T_{t5}) \eta_{mech} \quad (\text{eq. 5.2})$$

These equations determined the total temperature drop across the two turbine components given power required of the fan and compressor to meet mission analysis overall pressure ratio requirements.

Mission analysis determined a turbine inlet total temperature of 3400°R was required. The HPT spool rate

was selected based upon mass flow rates of the compressor, whereas the LPT spool rate was determined using an optimization routine based on the fan diameter provided in the RFP. The mass flow rate of fuel was assumed to be negligible compared to the mass flow rate of air, therefore the mass flow entering the turbine is the same as the mass flow leaving the compressor. The HPT inlet flow Mach was selected based on optimal burner exit Mach values specified in [5]. A modified specific heat model was assumed using a hot section value specified in the RFP. Initial blade mean radius was determined iteratively starting from the final compressor mean radius and increasing in quart-inch increments until a value was found which could facilitate the large stage total temperature differential without exceeding the AN^2 (A stress metric) range described in [5]. AEDsys sub-suite, TURBN was used in conjunction with hand calculations for all aerothermodynamic and flow analysis. The stage count was determined iteratively with consideration to known acceptable parameter ranges, overall length and weight requirements. TURBN was also used to sketch blade airfoil curves, disk and rim widths and flow areas. It is worth noting TURBN is not yet capable of accurate disk/rim sketches. The dimensions shown are not indicative of the complex geometry demanded by centrifugal stress considerations. All initial assumptions are displayed in table 5.1.

| Parameter | Values | | Units |
|-----------------------------|--------|--------|------------------------------------|
| | HPT | LPT | HPT/LPT |
| Number of Stages | 2 | 2 | - |
| Mass Flow Rate | 193.64 | 193.64 | $\frac{lbf}{s}$ |
| Spool Angular Velocity | 850 | 463 | $\frac{rad}{s}$ |
| Inlet Total Pressure | 242 | 42 | <i>psia</i> |
| Inlet Total Temperature | 3400 | 2380 | $^{\circ}R$ |
| First Stage Flow angle at 1 | 0 | 20 | <i>deg</i> |
| First Stage Mach at 1 | 0.4 | 0.75 | - |
| Ratio of Specific Heats | 1.33 | 1.33 | - |
| Gas Constant | 53.34 | 53.34 | $\frac{ft * lbf}{lbf * ^{\circ}R}$ |
| Hot Section Specific Heat | 0.2763 | 0.2763 | $\frac{Btu}{lbf * ^{\circ}R}$ |
| Mean Radius from Centerline | 18.75 | 18.75 | <i>in</i> |
| Mean Rotor Blade Velocity | 1328.1 | 926 | <i>ft/sec</i> |

Table 5.1 Turbine Design Assumptions

5.2 Turbine Flow Calculations

Velocity triangles were calculated through every stage of the turbine at the hub, mean radius and tip of the blade. Calculations were performed using AEDsys' TURBN program and verified by hand calculations.

For purpose of calculations, the Mach number was assumed to be known at the stator exit while the stator exit flow angle was assumed to be unknown. A stage by stage manual iterative process was used to decide upon a design. The design was finalized upon completing a configuration which met the power demands of the cold section turbomachinery, and fell within or close to acceptable ranges specified in [5], with some consideration to technological updates. Key items of interest included the angle of backward running flow, and the stator flow exit angle. Backward running flow, or exit swirl angle, is directly related to the work output of the stage where zero exit swirl constitutes maximum efficiency [20]. In the case of the CE18-Bullet design, increasing swirl angle led to a decrease in the number of component stages in both the HPT and the LPT due to the increase in stage output. For this reason, efficiency was slightly sacrificed in favor of material savings stemming from the reduction of stages. [5] and [20] agree that the stator exit angle should not exceed 70 degrees. At exit angles not exceeding 58 degrees, the velocity triangle calculations are well within reason. Design choices are displayed in table 5.2. Corresponding velocity triangle calculations are displayed in tables 5.3 and 5.4.

| Parameter | HPT | | LPT | | Units | Exit Guide Vane | | |
|------------|---------|---------|---------|---------|-------|-----------------|-------|-------|
| | Stage 1 | Stage 2 | Stage 1 | Stage 2 | | Parameter | Value | Units |
| U3/U2 | 0.92 | 0.94 | 0.942 | 0.93 | - | Zweifel | 1 | - |
| Mach @ 2 | 1.03 | 1.1 | 1.045 | 1.14 | - | | | |
| Alpha @ 3 | 18 | 20 | 17 | 18 | deg | Chord/Height | 0.3 | - |
| Tt3 | 2890 | 2380 | 2108 | 1836 | R | | | |
| Stator Z | 1 | 1 | 1 | 1 | - | Exit Flow Angle | 0 | deg |
| Rotor Z | 1 | 1 | 1 | 1 | - | | | |
| Stator c/h | 0.55 | 0.45 | 0.35 | 0.35 | - | Loss Coeff | 0.02 | - |
| Rotor c/h | 0.55 | 0.45 | 0.35 | 0.35 | - | | | |
| Stator phi | 0.02 | 0.02 | 0.02 | 0.02 | - | Exit Mach | 0.5 | - |
| Poly eff | 0.89 | 0.89 | 0.89 | 0.89 | - | | | |

Table 5.2 Turbine Design Choices

| HPT | | | | | | | | | |
|---------|-----------|------------|-------|-------|----------|----------------|---------------|----------|----------|
| | | Streamline | M | Mr | V (ft/s) | α (deg) | β (deg) | u (ft/s) | v (ft/s) |
| Stage 1 | Station 1 | hub | 0.4 | - | 1100 | 0 | - | 1100 | 0 |
| | | mean | 0.4 | - | 1100 | 0 | - | 1100 | 0 |
| | | tip | 0.4 | - | 1100 | 0 | - | 1100 | 0 |
| | Station 2 | hub | 1.064 | - | 2721 | 58.38 | - | 1427 | 2317 |
| | | mean | 1.03 | 0.657 | 2647 | 57.38 | 32.28 | 1427 | 2229 |
| | | tip | 0.999 | - | 2579 | 56.4 | - | 1427 | 2148 |
| | Station 3 | hub | 0.554 | - | 1388 | 18.91 | - | 1313 | 450 |
| | | mean | 0.551 | 0.874 | 1380 | 18 | 53.2 | 1313 | 427 |
| | | tip | 0.548 | 0.89 | 1374 | 17.17 | - | 1313 | 406 |
| Stage 2 | Station 1 | hub | 0.554 | - | 1388 | 18.91 | - | 1313 | 450 |
| | | mean | 0.551 | - | 1380 | 18 | - | 1313 | 427 |
| | | tip | 0.548 | - | 1374 | 17.17 | - | 1313 | 406 |
| | Station 2 | hub | 1.179 | - | 2732 | 60.05 | - | 1364 | 2367 |
| | | mean | 1.1 | 0.688 | 2579 | 58.08 | 32.28 | 1364 | 2189 |
| | | tip | 1.035 | - | 2451 | 56.19 | - | 1364 | 2037 |
| | Station 3 | hub | 0.612 | - | 1384 | 22.19 | - | 1282 | 523 |
| | | mean | 0.603 | 0.974 | 1364 | 20 | 54.46 | 1282 | 467 |
| | | tip | 0.596 | 1.01 | 1349 | 18.19 | - | 1282 | 421 |

Table 5.3 High Pressure Turbine Velocity Triangle Calculations

| LPT | | | | | | | | | |
|---------|-----------|------------|--------|-------|----------|----------------|---------------|----------|----------|
| | | Streamline | M | Mr | V (ft/s) | α (deg) | β (deg) | u (ft/s) | v (ft/s) |
| Stage 1 | Station 1 | hub | 0.755 | - | 1683 | 18.13 | - | 1599 | 524 |
| | | mean | 0.75 | - | 1672 | 17 | - | 1599 | 489 |
| | | tip | 0.746 | - | 1664 | 16 | - | 1599 | 459 |
| | Station 2 | hub | 1.103 | - | 2346 | 47.01 | - | 1600 | 1716 |
| | | mean | 1.045 | 0.804 | 2242 | 44.48 | 21.96 | 1600 | 1571 |
| | | tip | 0.99 | - | 2158 | 42.17 | - | 1600 | 1449 |
| | Station 3 | hub | 0.76 | - | 1593 | 18.92 | - | 1507 | 516 |
| | | mean | 0.751 | 0.976 | 1576 | 17 | 42.62 | 1507 | 461 |
| | | tip | 0.744 | 0.99 | 1563 | 15.43 | - | 1507 | 416 |
| Stage 2 | Station 1 | hub | 0.76 | - | 1593 | 18.92 | - | 1507 | 516 |
| | | mean | 0.751 | - | 1576 | 17 | - | 1507 | 461 |
| | | tip | 0.744 | - | 1563 | 15.43 | - | 1507 | 416 |
| | Station 2 | hub | 1.2243 | - | 2434 | 46.31 | - | 1682 | 1760 |
| | | mean | 1.14 | 0.897 | 2269 | 42.18 | 29.56 | 1682 | 1524 |
| | | tip | 1.07 | - | 2152 | 38.61 | 42.52 | 1682 | 1343 |
| | Station 3 | hub | 0.872 | - | 1683 | 21.66 | - | 1564 | 621 |
| | | mean | 0.85 | 1.097 | 1644 | 18 | 54.46 | 1564 | 508 |
| | | tip | 0.837 | 1.12 | 1622 | 15.37 | - | 1564 | 430 |

Table 5.4 Low Pressure Turbine Velocity Triangle Calculations

5.3 Turbine Aerothermodynamic Calculations

The aerothermodynamics at each stage of the high pressure turbine and low pressure turbine were calculated in conjunction with the design triangles. The total temperature differential across each stage is decided as a design choice allowing the corresponding pressure ratio, stage loading coefficients and degree of reaction to be calculated. The Mattingly text [5] specifies an acceptable stage loading coefficient range with an upward limit of three, and an acceptable flow coefficient range with upward limit of two. Additionally, [20] states that the degree of reaction should range from near purely impulsive at the hub to 50 % at the tip. For design choices summarized in table 5.2, the corresponding total temperatures, static temperatures, total pressures, static pressures, degrees of reaction and loading coefficients are shown in tables 5.5 and 5.6. All parameters fit squarely within their corresponding range of acceptable values. Material selection, which will be discussed in later section, determines that for the total temperatures at each stage, no cooling is needed.

| | | HPT Aerothermodynamics | | | | | LPT Aerothermodynamics | | | |
|---------|-----------|------------------------|---------|--------|----------|---------|------------------------|--------|----------|---------|
| | | Location | Tt (°R) | T (°R) | Pt (psi) | P (psi) | Tt (°R) | T (°R) | Pt (psi) | P (psi) |
| Stage 1 | Station 1 | hub | 3400 | 3313 | 242 | 217.9 | 2380 | 2175 | 42 | 29.23 |
| | | mean | 3400 | 3313 | 242 | 217.9 | 2380 | 2178 | 42 | 29.37 |
| | | tip | 3400 | 3313 | 242 | 217.9 | 2380 | 2180 | 42 | 29.48 |
| | Station 2 | hub | 3400 | 2865 | 239.7 | 120.2 | 2380 | 1982 | 41.59 | 19.9 |
| | | mean | 3400 | 2893 | 239.7 | 125.1 | 2380 | 2017 | 41.59 | 21.33 |
| | | tip | 3400 | 2919 | 239.7 | 129.7 | 2380 | 2043 | 41.59 | 22.49 |
| | Station 3 | hub | 2890 | 2751 | 115.9 | 95 | 2108 | 1925 | 24.24 | 16.8 |
| | | mean | 2890 | 2752 | 115.9 | 95.2 | 2108 | 1929 | 24.24 | 16.94 |
| | | tip | 2890 | 2754 | 115.9 | 95.4 | 2108 | 1931 | 24.24 | 17.04 |
| Stage 2 | Station 1 | hub | 2890 | 2751 | 115.9 | 95.01 | 2108 | 1925 | 24.24 | 16.8 |
| | | mean | 2890 | 2752 | 115.9 | 95.22 | 2108 | 1929 | 24.24 | 16.94 |
| | | tip | 2890 | 2754 | 115.9 | 95.39 | 2108 | 1931 | 24.24 | 17.04 |
| | Station 2 | hub | 2890 | 2351 | 114.7 | 49.9 | 2108 | 1680 | 23.98 | 9.6 |
| | | mean | 2890 | 2409 | 114.7 | 55.09 | 2108 | 1736 | 23.98 | 10.96 |
| | | tip | 2890 | 2456 | 114.7 | 59.52 | 2108 | 1773 | 23.98 | 11.94 |
| | Station 3 | hub | 2380 | 2241 | 48.1 | 37.79 | 1836 | 1631 | 12.97 | 8.05 |
| | | mean | 2380 | 2245 | 48.1 | 38.06 | 1836 | 1641 | 12.97 | 8.24 |
| | | tip | 2380 | 2248 | 48.1 | 38.26 | 1836 | 1646 | 12.97 | 8.35 |

Table 5.5 Turbine Aerothermodynamic Calculations

| | | HPT | | | LPT | | |
|---------|----------------|------|--------|--------|------|--------|--------|
| | Blade Location | °R | ψ | ϕ | °R | ψ | ϕ |
| Stage 1 | hub | 0.22 | 2 | 1.07 | 0.21 | 2.2 | 2.2 |
| | mean | 0.28 | | | 0.32 | | |
| | tip | 0.33 | | | 0.41 | | |
| Stage 2 | hub | 0.21 | 2 | 1.03 | 0.18 | 1.73 | 1.8 |
| | mean | 0.32 | | | 0.35 | | |
| | tip | 0.41 | | | 0.46 | | |

Table 5.6 Turbine Degree of Reaction and Loading Coefficient Calculations

5.4 Blade Design

AEDsys' TURBN program has the ability to calculate rotor and stator blade profile characteristics, spacing and count based off inputs of Zweifel coefficient, chord to height ratio and flow calculations. The chord to height ratio for each rotor and stator was manually selected based on general guidelines found in [6].

The tangential force per unit depth of blades spaced a distance s apart can be expressed used the following equation:

$$F_t = \frac{\rho u_i^2 s}{g_c} (\tan(\alpha_i) + \frac{u_e}{u_i} \tan(\alpha_e)) \quad (\text{eq.5.3})$$

The equation for the maximum tangential force that can be achieved efficiently is obtained when the inlet total pressure on the pressure side of a turbine blade remains at its initial value then drops to the exit static pressure at the trailing edge, and the total pressure on the suction side of the blade immediately drops to the exit static pressure and remains there for the length of the chord. This maximum tangential force is expressed as shown in equation 5.4 where c_x is the axial chord of the blade [5].

$$F t_{max} = \frac{\rho V_e^2 c_x}{2g_c} \quad (\text{eq. 5.4})$$

In the case of the CE18 Bullet, the Zweifel tangential force coefficient, defined as the ratio of tangential force to maximum tangential force, was set to one in order to optimize rotor blade and nozzle spacing in the turbine. The annulus area at any station of the turbine stages are a function of total

temperature, total pressure, Mach number, flow angle and mass flow parameter (MFP). Using the MFP, it is possible to back out the area at any station using the equation shown below [5].

$$A_i = \frac{\dot{m}\sqrt{T_{ti}}}{P_{ti} \cos(\alpha) MFP(M_i)} \quad (\text{eq. 5.5})$$

Table 5.7 contains a summary of blade design calculations for each stage of the LPT and HPT.

| | | Stage 1 | | | Stage 2 | | | EGV | | |
|-----|------------------------------|---------|------|-------|---------|-------|-------|------|-------|------|
| | Station | 1 | 2 | 3 | 1 | 2 | 3 | 1 | 2 | 3 |
| HPT | Turbine Axial Position (in) | 0 | 0.08 | 0.838 | 1.966 | 3.197 | 4.707 | - | - | - |
| | Blade length (in) | 1.22 | 1.3 | 1.42 | 1.93 | 2.8 | 4.03 | - | - | - |
| | Flow area (in ²) | 0.99 | 1.05 | 1.16 | 1.57 | 2.3 | 3.3 | - | - | - |
| LPT | Axial Position (in) | 0 | 0.75 | 1.372 | 3.678 | 6.14 | 8.76 | 9.74 | 11.43 | 12.5 |
| | Blade height (in) | 3.18 | 3.5 | 4.05 | 5.18 | 6.45 | 8.73 | 9.23 | 10.95 | 11 |
| | Flow area (in ²) | 3.33 | 3.75 | 4.23 | 5.42 | 6.75 | 7.37 | 8.5 | 9.13 | 11.4 |

Table 5.7 Turbine Blade Design Calculations

5.5 Turbine Material Selection

Material selection for the turbine disk and blades is of utmost importance. The HPT first stage presents a problem which is a hot topic in the research and development world. The forces which the turbine blades must endure are comparable to holding a blow-torch to a turbine blade while suspending a semi-truck from it. It is generally agreed that the temperature capability of nickel based metals for turbine blade application have reached their limit [30]. Silicon carbides have demonstrated high temperature mechanical properties making them a prime candidate for the next generation of turbine blade material, however, oxygen and water vapor cause the ceramics to quickly corrode, degrading its superior properties [31]. For this reason, it is critical that the silicon carbide substrate be coated with a substance that acts as both an environmental barrier to prevent degradation and a thermal barrier to keep the substrate below its 2800 °R temperature limit. As of 2017, NASA Glenn Research Center Materials and Structures Division has indicated successful development of state of the art, fifth generation silicon carbide substrate with an EBC consisting of HfO_2 rare earth silicates, a bond coat consisting of $HfO_2Si - x$, and an advanced top coat. This is claimed to be capable of withstanding temperatures exceeding 3460 °R [32].

With the CE18-Bullet's incredibly high turbine inlet temperature of 3400 °R, the hot section materials must be nothing short of cutting edge. Disk and rim materials will be constructed from advanced nickel superalloys with low thermal expansion coefficients in order to mitigate low-cycle fatigue, and blades will be 5th generation silicon carbide ceramics with thermal/environmental barrier coatings. Current technology is largely un-proven, however, with an anticipated service entry limit of 2025, there is plenty of time for further testing and verification of 5th generation materials.

5.6 Stress Considerations

Reference texts [6] and [20] both use AN^2 as a metric for blade stress considerations where 'A' is annulus area and $N = \omega \left(\frac{30}{\pi}\right)$. As a rule of thumb, AN^2 should be no more than $5 \times 10^{10} \text{ in}^2 \text{ rpm}^2$. The values of AN^2 were calculated for each stage of the HPT and LPT and are tabulated in table 5.9.

A stress analysis was performed to ensure blade structure was able to withstand the immense forces that accompany high spool angular velocity rates. The material properties for silicon carbide used in the analysis were as found in [33] and are displayed in table 5.8. The following equation be used to calculate centrifugal stress imposed on turbine blades [5]:

| | |
|--|----------|
| $\frac{\text{lbm}}{\text{ft}^3}$ Density, ft^3 | 1.94E+02 |
| Tensile Strength, psi | 3.92E+08 |
| Modulus of Elasticity, psi | 6.00E+07 |
| Thermal Expansion Coeff, $\frac{1}{^\circ\text{R}}$ | 5.56E-07 |

Table 5.8 Silicon Carbide Properties

$$\sigma_c = \frac{\rho\omega^2 A}{4\pi} \left(1 + \frac{A_t}{A_h}\right) \quad (\text{eq. 5.6})$$

Where 'A' is the cross sectional flow area, ω is spool angular velocity and the ratio of A_t to A_h is the blades taper ratio. Using this equation, the centrifugal stresses and the corresponding margins of safety for rotating components in each stage were determined. The results are shown in table 5.9.

| | Component | AN^2 (in^2rpm^2) | Centrifugal stress (psi) | Margin of Safety |
|-----|-----------|------------------------|--------------------------|------------------|
| HPT | Stator | | - | - |
| | Rotor | 1.10E+10 | 7405 | 51.8 |
| | Stator | | - | - |
| | Rotor | 2.18E+10 | 3916 | 23.7 |
| LPT | Stator | | - | - |
| | Rotor | 1.19E+10 | 7719 | 49.73 |
| | Stator | | - | - |
| | Rotor | 1.90E+10 | 13010 | 29.09 |

Table 5.9 Turbine Blade Stress Analysis

Although the analysis uses strengths of Sic/Sic CMCs at room temperature, [34] states in his presentation that Glenn Research Center materials division has proven the ability for CMCs to maintain their mechanical properties through temperatures in upwards of 3400 °R. Analysis shows that components are well within the bounds of safety with all highly positive margins of safety, and AN^2 values well below the 5×10^5 limit.

5.7 Turbine Model

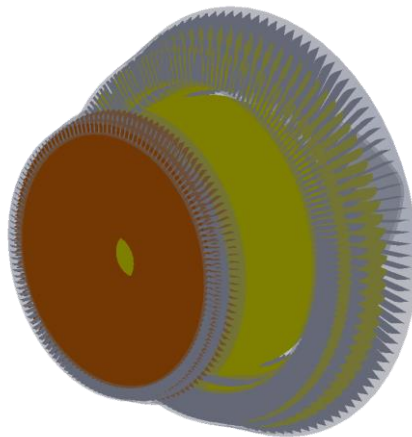


Figure 5.2 Turbine (HPT and LPT) CAD Model

6.0 Mixer Design

Aft of the turbine the core-flow is rejoined by the bypass-flow. To promote the mixing between the core and bypass flows, a forced mixer with scalloped lobes will be used. Scalloped lobe mixers with a relatively high number of lobes and higher lobe penetration have been found to reduce engine noise at high thrust level [35]. A summary of the mixer design is shown in the table below.

| Parameter | Value |
|---------------|-------|
| # of Lobes | 20 |
| Length (in) | 18.5 |
| Diameter (in) | 68.5 |

Table 6.1 Mixer Design Parameters

To assist in nozzle design, which will be covered in the next section, the flow properties aft of the mixer were determined. Using a mass weighted average of the bypass and core flow the table below shows calculations to simulate a fully mixed exhaust flow.

| | Mass Flow | Total Pressure | Total Temp. | Velocity |
|--------|-------------|----------------|-------------|------------|
| Core | 193.6 lbm/s | 11.82 psi | 1745 R | 1498 ft/s |
| Bypass | 406.7 lbm/s | 14.93 psi | 785.6 R | 689.7 ft/s |
| Mixed | 600.3 lbm/s | 13.93 psi | 1095 R | 950.4 ft/s |

Table 6.2 Mixer Flow Calculations

7.0 Exhaust System Design

The following section will detail the design of a converging-diverging nozzle for the CE18-Bullet as well as a preliminary design for the afterburner.

7.1 Nozzle Type Selection

The nozzle is an axisymmetric, converging-diverging nozzle with a variable geometry. The nozzle varies both mechanically and aerodynamically by using blow-in doors at subsonic speeds to prevent overexpansion losses. At supersonic speeds the nozzle acts as if it has a fixed ejector area. Mechanical and aerodynamic ejectors were considered individually, but the additional weight for mechanical alone and the aerodynamic ejectors need for a fixed throat area ruled them both out. Converging-diverging was the obvious choice for supersonic, due to its ability to expand to the ambient pressure. Axisymmetric was chosen over 2D because the candidate engine isn't considering any form of thrust vectoring, so axisymmetric minimizes complexity [36].

7.2 Nozzle Sizing

The mixer flow calculations from table 6.2 were used as inputs for the AEDsys nozzle design tool. To begin the nozzle design the converging and diverging nozzle angles were meticulously selected. The converging section, which brings the flow up to a sonic condition at the throat, cannot have too steep an angle. If the angle is too steep, the discharge coefficient will be low. The divergent angle cannot be too high, as well. A high divergent angle causes higher likelihood of flow separation as well as a lower angularity coefficient, which means that the flow is providing less longitudinal force per mass exiting the nozzle. However, low angles for the converging and diverging sections means that the nozzle grows in length and weight. Therefore, the lowest angles were selected while still maintaining a high level of performance. The divergence angle was chosen according to figure 7.1. A corresponding exit-to-throat area ratio was chosen to provide the highest gross thrust coefficient.

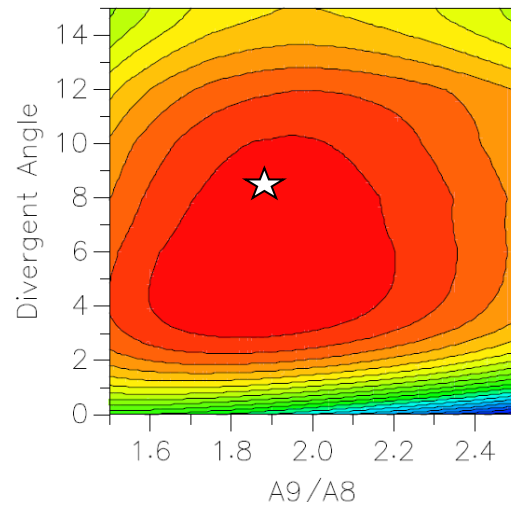


Figure 7.1 Gross Thrust Coefficient contour plot

The nozzle angles as well as the nozzle area ratio are shown in the table below.

| Convergent Angle | Divergent Angle | A9/A8 |
|------------------|-----------------|-------|
| 10 degrees | 8 degrees | 1.89 |

Table 7.1 Nozzle Angles and Sizing

7.3 Nozzle Design Results

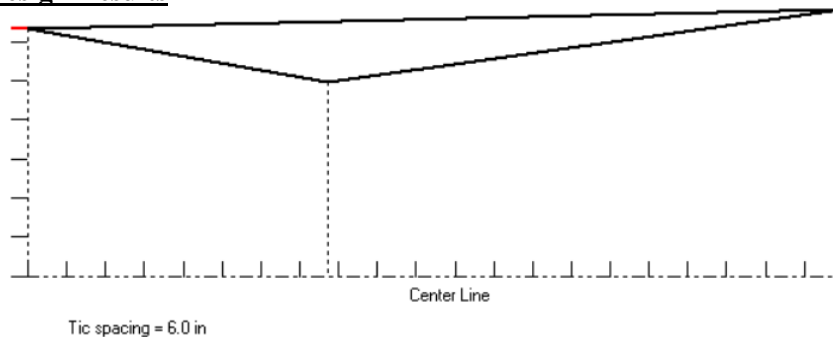


Figure 7.2 Nozzle On-Design Cross Section

| Mach@9 | Velocity@9 | Exit Pressure Ratio | Gross Thrust | Discharge Coeff. | Angularity Coeff. | Velocity Coeff. | Gross Thrust Coeff. |
|--------|------------|---------------------|--------------|------------------|-------------------|-----------------|---------------------|
| M9 | V9 (ft/s) | P9/P0 | F (lbf) | C _D | C _A | C _V | C _{fg} |
| 2.095 | 2522.0 | 1.0046 | 46,817 | 0.9763 | 0.9942 | 0.9952 | 0.9659 |

Table 7.2 On-Design Nozzle Output Properties

The resulting velocity and gross thrust do not account for the fact that the aircraft is moving. Therefore the absolute velocity of the exhaust flow relative to the ground is actually the aircraft’s velocity subtracted from the listed V9. Likewise, the gross thrust needs to be corrected for the aircraft velocity, producing a net thrust of 18,140 pounds.

7.4 Afterburner Design

From the mission analysis, using the given aircraft information from the RFP, it was determined from AEDsys that the CE18-Bullet would require an afterburner during the high drag transonic pinch. However, the CE18-Bullet as shown in table 1.5 exceeds the required thrust for the transonic pinch. Regardless of this discrepancy, to ensure a fully capable engine, the CE18-Bullet was designed with an afterburner.

The afterburner dimensions are shown in table below.

| Parameter | Value |
|---------------|-------|
| Length (in) | 90 |
| Diameter (in) | 76 |

Figure 7.3 Afterburner Geometry

7.5 Exhaust System Model

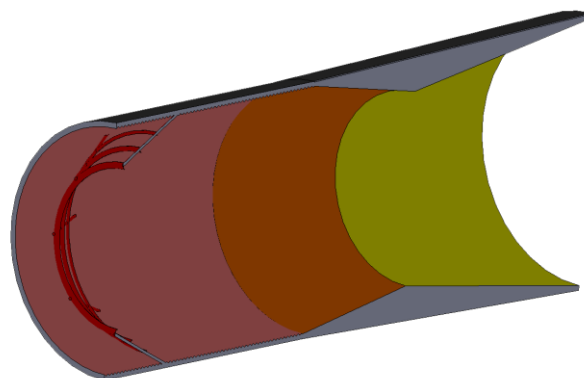


Figure 7.3 Afterburner and Nozzle CAD Model

8.0 CE18-Bullet Flowpath

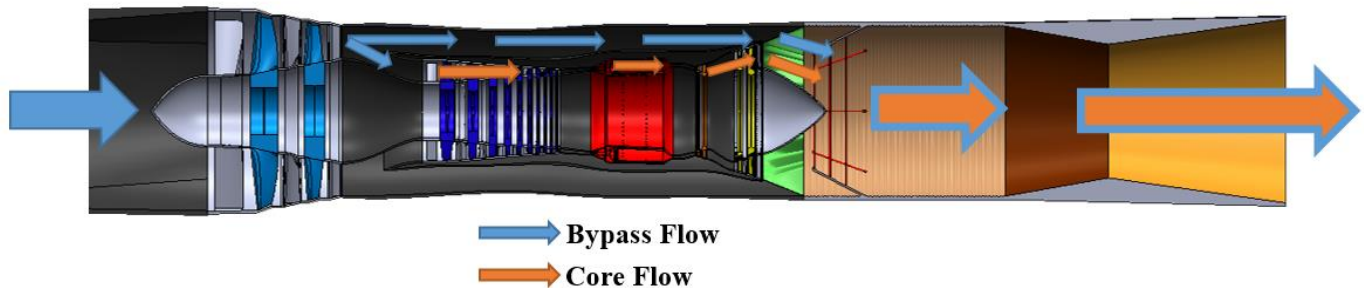


Figure 8.1 CE18-Bullet Flowpath

9.0 Engine Subsystems

9.1 Auxiliary Power Unit and startup

The CE18-Bullet will use a standard auxiliary power unit (APU) delivering pneumatic through an air turbine starter to provide shaft power to the compressor to initiate the engine main systems. Once the compressor has spun up to provide adequate flow to the combustor, the engine will start.

9.2 Fuel System

Like most modern engines, the CE18-Bullet will make use of an electronically controlled fuel system with a manual backup in case of electrical failure. The fuel system will draw the fuel from the tanks to a high pressure pump to inject into the combustor or afterburner.

9.3 Engine Control

Modern and near future transportation aircraft make use of Full Authority Digital Engine Control. The CE18-Bullet will be no different; implementing a FADEC to allow for a smoother control of the engine. Using monitors on different aspects of the engine, the FADEC allows the engine to be controlled at an optimal efficiency for each input.

9.4 Bearing

In order to have long lasting and stable turbomachinery, bearings need to be investigated. The CE18-Bullet engine will make use of steel bearings over magnetic due to the high complexity and power

needed for magnetic bearings. Using steel bearings means that an additional lubrication system will need to be installed, however the simplicity of the steel design allows for less overall space and weight as opposed to magnetic. The mechanical losses associated with steel bearings are a justified tradeoff for the reliability and simplicity of the system.

10.0 Design Summary and Considerations

To recap, the CE18-Bullet supersonic engine is a two spool, mixed flow, afterburning low-bypass turbofan. This design not only meets, but surpasses the requirements of TSFC and thrust at all flight regimes. The CE18-Bullet is small enough to integrate into the proposed airframe design and provides adequate performance metrics to push the flight envelope even further. The classical design of CE18-Bullet gives confidence that the maintainability and reliability will be on par with engines in service today.

Considering the design discussed in this report, and the implications thereof, the CE18-Bullet supersonic engine is an excellent candidate for a next generation supersonic transport. The classical design coupled with the integration of near future materials and systems allow for a next generation engine capable of powering a fleet of aircraft for the future.

11.0 Constraint Diagram

Given the limited knowledge on the airframe, a constraint diagram based on cruise, LTO, and a service ceiling was constructed. The AEDSys software 'constraint' tool was used to produce a constraint plot. Using values for cruise Mach and altitude, as well as Mach at LTO and takeoff distance, the following plot was produced.

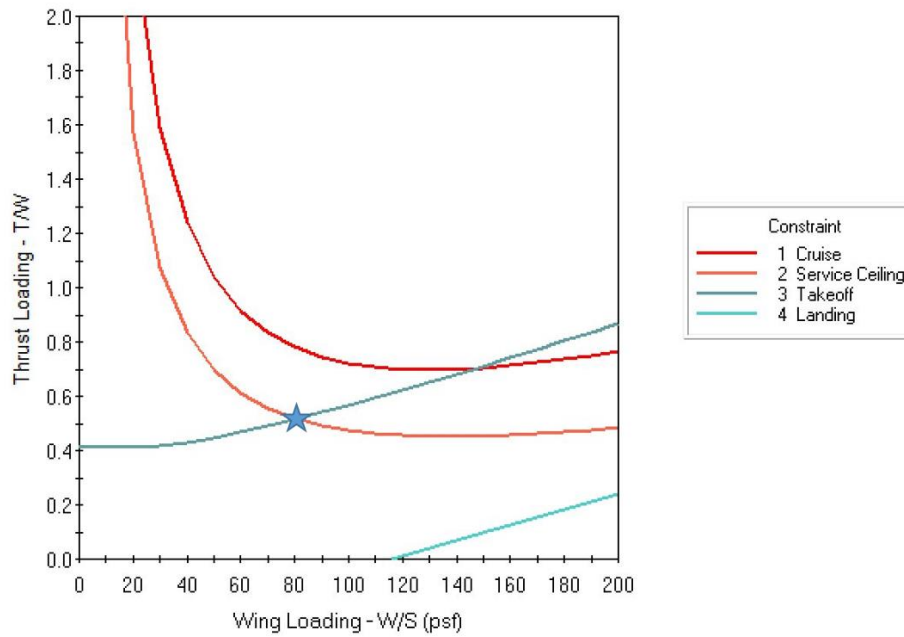


Figure 11.1 Constraint Diagram

12.0 CE18-Bullet Full Engine Model

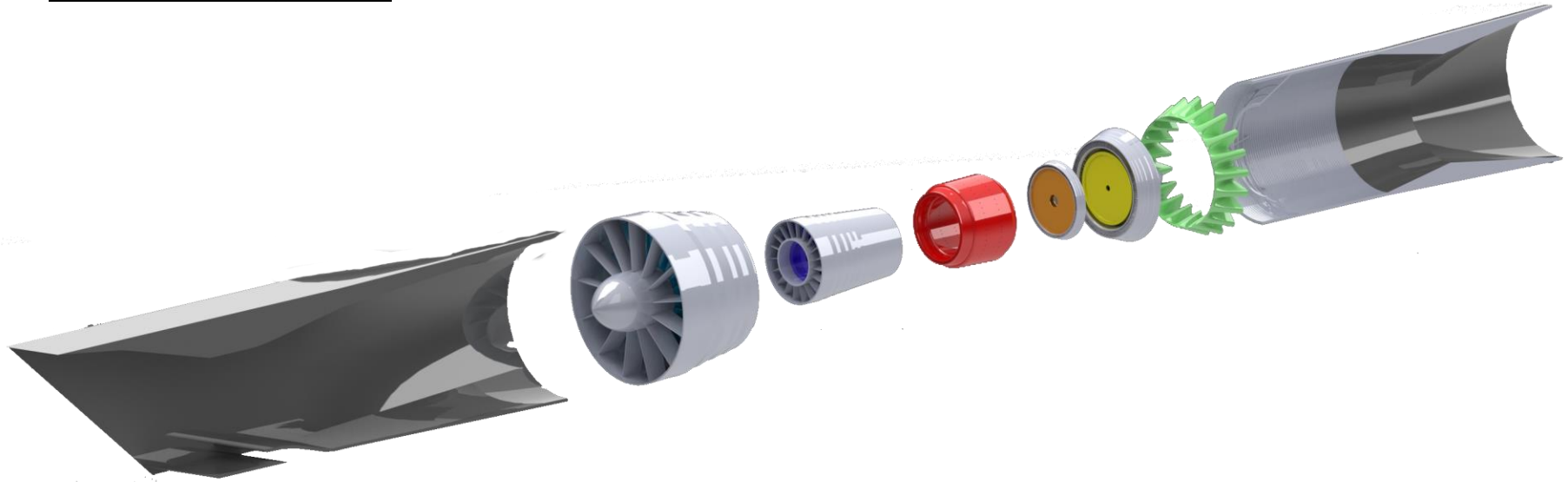


Figure 12.1 CE18-Bullet Exploded View

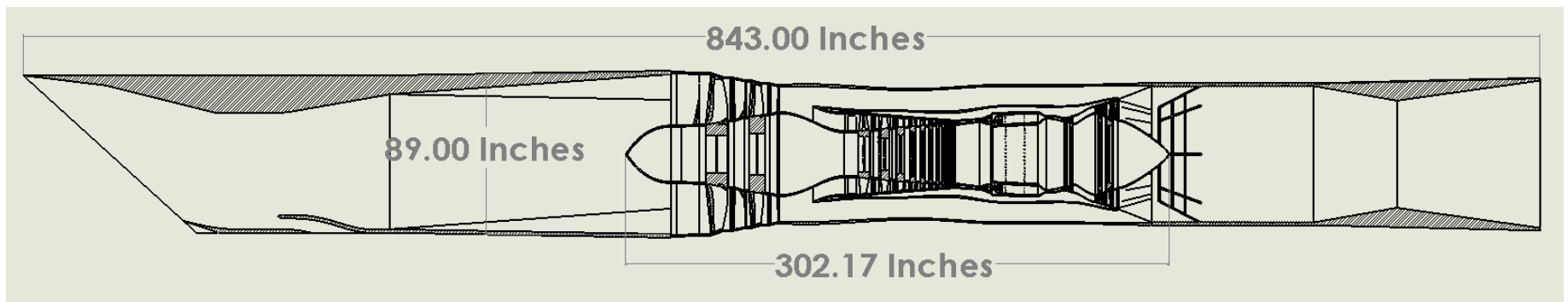


Figure 12.2 CE18-Bullet Drawing with Major Dimensions

13.0 References

- [1] "Candidate Engines for a Next Generation Supersonic Transport." *American Institute of Aeronautics and Astronautics*, 2017, doi:<https://www.aiaa.org/2018UndergradTeamEngine%E2%80%9393SupersonicTransport/>.
- [2] Welge, Harry, et al. "N+2 Supersonic Concept Development and Systems Integration." NASA, 2010.
- [3] *Supersonic transport*. (2018). *En.wikipedia.org*. Retrieved 26 April 2018, from https://en.wikipedia.org/wiki/Supersonic_transport
- [4] Kurzke, Joachim. "The Mission Defines the Cycle: Turbojet, Turbofan and Variable Cycle Engines for High Speed Propulsion." NATO Science and Technology Organization, doi:<https://www.sto.nato.int/publications/.../RTO-EN-AVT-185/EN-AVT-185-02.pdf>
- [5] Mattingly, Jack D., et al. *Aircraft Engine Design (2nd Edition)*. American Institute of Aeronautics and Astronautics, 2002.
- [6] Mattingly, Jack D., et al. *Elements of Propulsion: Gas Turbines and Rockets*. American Institute of Aeronautics and Astronautics, Inc., 2016.
- [7] Chati, Yashovardhan S, and Hamsa Balakrishnan. "Analysis of Aircraft Fuel Burn and Emissions in the Landing and Take Off Cycle Using Operational Data." ICRAT, 2014.
- [8] "General Electric F101." Wikipedia, Wikimedia Foundation, 8 May 2018, en.wikipedia.org/wiki/General_Electric_F101.
- [9] Crocker, Malcolm J. *Handbook of Acoustics*. Wiley, 1998.
- [10] Depuru Mohan, N. K, and M J Doty. "Active Chevrons for Jet Noise Reduction." International Congress On Sound and Vibration, 2017.
- [11] Berton, Jeffrey J, et al. "An Analytical Assessment of NASA's N+1 Subsonic Fixed Wing Project Noise Goal." American Institute of Aeronautics and Astronautics.
- [12] Padva, Eugenia. "Sound Absorption/Liner." DLR Portal, Institute of Propulsion Technology, www.dlr.de/at/en/desktopdefault.aspx/tabid-9004/15550_read-38382/.
- [13] "ICAO Aircraft Engine Emissions Databank." EASA, www.easa.europa.eu/easa-and-you/environment/icao-aircraft-engine-emissions-databank.
- [14] Kyprianidis K.G. Future Aero Engine Designs: An Evolving Vision. In: Benini E., editor. *Advances in Gas Turbine Technology*, Rijeka, Croatia: InTech; 2011
- [15] Kyprianidis, Konstantinos, et al. "A NOx Emissions Correlation for Modern RQL Combustors." *ICAE*, 2015.
- [16] Berton, Jeffery J, et al. "An Analytical Assessment of NASA's N+1 Subsonic Fixed Wing Project Noise Goal." NASA, 2009, citeseerx.ist.psu.edu/viewdoc/download?doi=10.1.1.453.546&rep=rep1&type=pdf.
- [17] H. Ran and D. Mavris, "Preliminary Design of a 2D Supersonic Inlet to Maximize Total Pressure Recovery," *AIAA 5th ATIO and 16th Lighter-Than-Air Sys Tech. and Balloon Systems Conferences*, 2005.

- [18] A. Sóbester, "Tradeoffs in Jet Inlet Design: A Historical Perspective," *Journal of Aircraft*, vol. 44, no. 3, pp. 705–717, 2007.
- [19] I. D. V. Faro, *Supersonic inlets*. Paris: Advisory Group for aerospace research and development, 1965.
- [20] Farokhi, S, "Aircraft Propulsion." 2nd Edition, John Wiley & Sons Ltd, West Sussex, United Kingdom, 2014.
- [21] Chestnutt, David, and John L Crigler. "Potential of Inlet Guide Vane Configuration for Inlet Noise Reduction." NASA, ntrs.nasa.gov/archive/nasa/casi.ntrs.nasa.gov/19690002230.pdf.
- [22] Neal, D. R. (2010). *The effects of rotation on the flow field over a controlled-diffusion airfoil* (Order No. 3458544). Available from ProQuest Dissertations & Theses Global. (871194240).
- [23] Salchow, K. *Forsch Ing-Wes* (1997) 63: 161. <https://doi.org/10.1007/PL00010825>
- [24] Kopeliovich, Dmitri "Materials Engineering." *Sintering of Ceramics [SubsTech]*, SubsTech, 3 June 2012, substech.com/dokuwiki/doku.php?id=typical_silicon_carbide_matrix_composite_reinforced_by_sic_long_fibers.
- [25] Portmann, R W, et al. "Stratospheric Ozone Depletion Due to Nitrous Oxide: Influences of Other Gases." The Royal Society, 2017, pdfs.semanticscholar.org/e313/67519f4301a50c0c0a5083319ed184f8f356.pdf.
- [26] Samuelsen, Scott. "Rich Burn, Quick Mix, Lean Burn (RQL) Combustor." netl.doe.gov/File%20Library/Research/Coal/energy%20systems/turbines/handbook/3-2-1-3.pdf.
- [27] Muktinutalapati, Nageswara Rao. "Materials for Gas Turbines – An Overview ." VIT University - India, cdn.intechweb.org/pdfs/22905.pdf
- [28] Halbig, Michael C. "Evaluation of Ceramic Matrix Composite Technology for Aircraft Turbine Engine Applications." NASA, pdfs.semanticscholar.org/8950/6f1a4be247a98e89fa870902435aa6bfc254.pdf.
- [29] Cho H H, Rhee D H. Local heat/mass transfer measurement on the effusion plate in impingement/effusion cooling systems. *Journal of Turbomachinery* 2001; 123(3): 601-608.
- [30] Lee, Kang N., et al. "Rare Earth Silicate Environmental Barrier Coatings for SiC/SiC Composites and Si₃N₄ Ceramics." *Journal of the European Ceramic Society*, vol. 25, no. 10, 2005, pp. 1705–1715., doi:10.1016/j.jeurceramsoc.2004.12.013.
- [31] Xu, Yue, et al. "Rare Earth Silicate Environmental Barrier Coatings: Present Status and Prospective." *Ceramics International*, vol. 43, no. 8, 2017, pp. 5847–5855., doi:10.1016/j.ceramint.2017.01.153.
- [32] Zhu, Dongming. *Advanced Environmental Barrier Coating Development for SiC/SiC Ceramic Matrix Composites: NASA's Perspectives*. Materials and Structures Division NASA Glenn Research Center, 9 Mar. 2016
- [33] Zinkle, S.J, Snead, L.L. *Thermophysical and Mechanical Properties of SiC/SiC Composites*. Oak Ridge National Laboratory. 1998.
- [34] Zhu, Dongming, et al. "Thermal Conductivity and Stability of HfO₂·Y₂O₃ and La₂Zr₂O₇ Evaluated for 1650°C Thermal/Environmental Barrier Coating Applications." *Advances in Ceramic Matrix Composites*

IX, 2012, pp. 329–343., doi:10.1002/9781118406892.ch23.

[35] Mengel, Vinod G, and William N Dalton. “Lobed Mixer Design for Noise Suppression.” NASA, ntrs.nasa.gov/archive/nasa/casi.ntrs.nasa.gov/20020070655.pdf.

[36] D. Migdal and J. J. Horgan, “Thrust Nozzles for Supersonic Transport Aircraft,” *ASME 1963 Aviation and Space, Hydraulic, and Gas Turbine Conference and Products Show*, Mar. 1963.